CENTRO BRASILEIRO DE PESQUISAS FÍSICAS

Amanda Nicotina Pereira

Implementation of Shortcuts to Adiabaticity via NMR.

Rio de Janeiro
March 16, 2018

Amanda Nicotina Pereira

Implementation of Shortcuts to Adiabaticity via NMR

Dissertação apresentada ao curso de Pós-Graduação em Física do Centro Brasileiro de Pesquisas Físicas, como requisito parcial para a obtenção do Título de Mestre em Física.

Orientador:
Prof. Dr. Roberto Sarthour

March 16, 2018

Agradecimentos

Gostaria de agradecer, primeiramente, a minha família. Nonno, Nonna e minha mãe Ana Paula por terem sempre feito tudo por mim. Inclusive terem feito possível ter ido pra faculdade e fazer o mestrado. Minha tia Antonella, por sempre poder conversar sobre qualquer que seja o assunto juntas. E aos amores da minha vida, meu irmão Paolo e minhas primas Anna Barbara, Millena e Nicole.

Quero agradecer, agradecer muito, a família que eu escolhi. Minha melhor amiga e irmã Flora por, literalmente, uma vida inteira de apoio e amizade. À Nina, por ser essa parceira em qualquer que seja a situação, por estar sempre do meu lado, reclamando, bebendo, rindo e fazendo as melhores/piores piadas que existem. Ao Rodrigo Bruni, por ser a pessoa mais louca que eu já conheci rs apesar de furão, meu grande amigo que vem nessa jornada da Física junto comigo desde o começo. Essa dissertação só foi possível por vocês.

Aos meus amigos de graduação Vinícius, Kainã, Tamara, Foster, Arthur, Renato e Arouca (um agradecimento especial por ter me ajudado a corrigir o texto) por todos os perrengues que passamos juntos naquele Fundão. Fico muito feliz da nossa amizade se manter até hoje. E ao Gabriel que inferniza minha vida todos os dias até hoje.

Ao pessoal do CBPF, Guilherme, Pedro Caneda, Felipe, Ivana, Josi, Dani, Erich, Zé, Leo, André e Guilherme Bremm. Agradeço também ao pessoal da limpeza do sexto andar, Sheila, Maria e Ismael, pelas conversas descontraídas no refeitório e por sempre me emprestarem o sal! Agradeço também a alguns seguranças do CBPF, principalmente ao André, por ter se preocupado e agido como um amigo num momento muito delicado.

Ao Prof. Roberto Sarthour, orientador deste trabalho, pelo apoio durante esta etapa tão importante. Ao Prof. Alexandre Souza por ter me ajudado nos experimentos que não foram nada fáceis. Ao Prof. Fernando de Melo por um curso de Mecânica Quântica incrível e ao Prof. Ivan Oliveira por ter me dado a oportunidade de ser monitora do curso de Mecânica Quântica, foi uma experiência trabalhosa porém pude aprender muito.

Ao bar Águia dos Andes, principalmente ao Rafa, por sempre separar uma mesa com uma Antártica gelada, um otimo antendimento e aquela saideira por conta da casa de lei.

Contents

Resumo **iv**

Abstract **v**

1 Introduction **1**

2 Quantum information via NMR systems **3**

2.1 Quantum Information 3

2.1.1 Qubits 3

2.1.2 Quantum Gates 7

2.1.3 Quantum Simulations 8

2.1.4 Comparing Quantum States 9

2.2 An introduction to NMR 10

2.2.1 Spins as Qubits 12

2.2.2 The Classical Approach 13

2.2.3 The Quantum Approach 15

2.2.4 Bloch Equations 16

2.3 Experimental Apparatus 18

2.3.1 Radio-Frequency Pulses 18

2.3.2 Relaxation and Spin Echo 20

2.4 Quantum State Tomography 22

2.4.1 State Representation 23

2.4.2 Quantum State Tomography via NMR 24

3 Shortcuts to Adiabaticity **27**

3.1 Adiabatic Theorem 27

3.1.1 Berry's phase 30

3.2 Counter-Adiabatic Hamiltonian 30

3.3 Shortcuts via RMN 32

3.3.1 Generalized Non-Transitional Evolutions 33

3.3.2 Optimal Non-Transitional Evolutions 34

3.3.3 Adiabatic Phase Non-Transitional Evolutions 34

3.4 Resonance Condition . . . 35

4 Shortcuts to Adiabaticity via NMR **37**

4.1 Calibration and Relaxation . . . 37
  4.1.1 Sample . . . 38
  4.1.2 Initial Set Up . . . 38
  4.1.3 Calibration . . . 39
  4.1.4 T_1 and T_2 . . . 40
4.2 Experimental Implementation . . . 41
  4.2.1 Initial State . . . 41
  4.2.2 Shaped Pulses . . . 43
  4.2.3 Implementation . . . 45
  4.2.4 State Comparison . . . 46
4.3 Analysis . . . 47

5 Conclusion **50**

Resumo

Neste trabalho desenvolvemos uma breve introdução à teoria de Informação Quântica definindo qbits, portas lógicas quânticas e simulações quânticas. Também tratamos da Ressonância Magnética Nuclear (RMN), e como implementar qbits usando spins nucleares, que são sistemas de dois níveis que satisfazem as condições necessárias para serem implementados como tais. Em seguida, tratamos do teorema adiabático e a derivação de atalhos que implementam evoluções adiabáticas sem o vínculo temporal. Vemos que em sistemas que possuem condição de ressonância, como a RMN, quando nessa condição, o teorema adiabático não é suficiente para garantir uma evolução adiabática. Por fim, descrevemos os procedimentos padrões para realizar experimentos em RMN. Também descrevemos como os experimentos foram feitos para comprovar que esses atalhos, de fato, implementam evoluções adiabáticas mesmo quando a condição para adiabaticidade é violada.

Abstract

In this work, we develop a brief introduction to Quantum Information theory defining qbits, quantum logic gates and quantum simulations. We also discussed Nuclear Magnetic Resonance (NMR) and how to implement qubits using nuclear spins, which are two-level systems that satisfy the necessary conditions to be implemented as such. Moreover, we talked about the adiabatic theorem and the derivation of shortcuts that implement adiabatic evolutions without the temporal constraint. We show that in systems with a resonance condition, such as NMR, when in this condition, the adiabatic theorem is not sufficient to guarantee an adiabatic evolution. Finally, we described the standard procedures to perform NMR experiments and how the experiments were done to prove that, indeed, these shortcuts implement adiabatic evolution even when the adiabatic condition is violated.

Chapter 1

Introduction

The idea of a Quantum Computer (QC) was first introduced in the early 1980s [1] [2]. A QC is a computer that operates by the laws of Quantum Mechanics and, its advantage is the possible optimization of computational problems [3]. What is responsible for the QC supremacy over classical computation are the intrinsic quantum mechanical phenomena, such as, entanglement and state superposition. Algorithms were developed for the implementation in the QC, for example, Shor's algorithm for quantum discrimination [4], the Deutsch-Jozsa algorithm for constant/balanced functions [5] and the Grover algorithm for database search [6]. One of the greatest challenges in quantum computation is its experimental implementation, because quantum states are submitted to decoherence [7] when not perfectly isolated from the environment. However, some physical systems fulfill the requirements for the QC implementation. It has been shown that the NMR technique is suitable for implementing quantum algorithms and unitary quantum evolutions. Indeed, experiments with over 10 qubits were performed using this technique [8]. What makes a NMR experiment act like a QC is the possibility of manipulating the quantum states of nuclear spins. These nuclear spins can be mapped into a two-level system, a qubit. One of the biggest advantages of quantum computation via NMR is the typical relaxation times for the nuclear systems. They are large when compared with the times necessary for the implementation of unitary evolutions. The manipulation of the spin systems is given by the application of a radio frequency (RF) sequence of pulses and, it is with this RF sequence that the unitary transformation of the spin system happens [9]. After the implementation of the spin system dynamics, the readout is equally important. This task is often done by performing a Quantum State Tomography (QST) in the system [10].

The adiabatic theorem states that, given an initial eigenstate of an Hamiltonian $\mathcal{H}(t)$, the adiabatic evolution will always be given in an eigenstate of this Hamiltonian. Provided that the evolution varies sufficiently slowly [11], [12], [13]. Therefore, the adiabatic evolution can be seen as a transition-less evolution. However, implementing this adiabatic dynamics can be problematic [14]. This is given because the requirement of slow varying Hamiltonians provide sufficient time for the decoherence effects act on the system. In this dissertation, we will work with *Shortcuts to Adiabaticity*, which is a technique to perform an adiabatic dynamics without the time constraint. Shortcuts to adiabaticity are alternative processes that can reproduce the same final state as the adiabatic process in a finite, shorter time. Then, we are focused on finding a Hamiltonian that implements the evolution. This shortcuts were first introduced by M.V. Berry in 1987 [15]. They can be implemented by introducing the concept of a Counter-Adiabatic Hamiltonian, which is a Hamiltonian that when added to the original $\mathcal{H}(t)$ implements an evolution that behaves like an adiabatic one. Until now we only considered non-transitional evolutions, that is, evolutions without change in the energy levels. However, generalized non-transitional evolutions allow us control over the phases that go with the evolutions [16]. This means that we can build an optimal Hamiltonian, when it comes to energy cost.

Therefore, the scope of this work is to verify experimentally that these shortcuts actually mimic an adiabatic evolution using the NMR technique to do so. The verification of the shortcuts using the generalized non-transitional evolution has not been done in the NMR architecture.

This dissertation is presented as follows, in Chapter 2 there is a review on quantum information. Defining qubits, quantum gates and how quantum simulations are done. In addition, an introduction on NMR theory, showing the classical approach and the quantum approach for the motion of the nuclear spins. Bloch's equations, which are a phenomenological description of the bulk magnetization, were introduced. Lastly, a description of the experimental apparatus and a brief introduction on how to manipulate nuclear spin with RF pulses.

In Chapter 3, we introduced the adiabatic theorem and the adiabatic condition. Moreover, using Berry's phase we described a quantum state in the eigenvector basis, where the control over this state was made by the phases that accompany the evolution. Further, using the adiabatic evolution operator we found an expression for the Hamiltonian that mimics the adiabatic evolution and, thus, the counter-adiabatic Hamiltonian. This is the Hamiltonian that when added to the original $\mathcal{H}(t)$ gives the shortcut. At last, we took the NMR Hamiltonian and found using non-transitional evolutions and generalized non-transitional evolutions two Hamiltonian, $\mathcal{H}_{SA}^{op}(t)$ and $\mathcal{H}_{SA}^{ad}(t)$, that mimic the adiabatic evolution given by $\mathcal{H}_{NMR}(t)$.

In Chapter 4, the experimental details were explained and the results disclosed. The spectrometer description, how the calibrations and the relaxation times measurements were performed. Further, the experimental implementation of the Shortcuts was explained with the introduction of the modulation of RF pulses, the shaped pulses technique. Moreover, the experimental results were presented.

In Chapter 5, we conclude this dissertation and discuss future implementations of the techniques used in this work.

Chapter 2

Quantum information via NMR systems

In the beginning of the 1980s the scientific community was convinced that simulating Quantum Mechanics problems was a challenging task. The first difficulty is the exponentially growing amount of computation memory to save a physical quantum state. Besides, simulating temporal evolution requires a number of operations that also grows exponentially. Therefore, these problems can not always be treated by classical computation. In 1985 Richard Feynman introduced the concept of a quantum computer that could solve the problem [1]. This machine would have the capacity of containing an exponential quantity of information without using the same exponential amount of physical resource; making quantum simulations a natural application.

Over a decade later, in 1996 [17], it was shown that a quantum computer, which is a well defined qubit set that can be initialized, measured and that quantum gates can be implemented using it, can act like an universal quantum mechanical simulator. However, a quantum computer is not always needed to simulate a quantum evolution. For simpler simulations, simpler quantum devices that imitate the evolution of other quantum systems can be used. We believe that, in the future, practical quantum simulations may become a reality before the actual quantum computer.

2.1 Quantum Information

2.1.1 Qubits

Classical computation is built upon the use of *bits*. In the same way, quantum computation is built upon a physical object called *quantum bit* or *qubit*. In spite of being an actual physical object, a *qubit* can also be treated as a mathematical object. As a consequence, a quantum information theory can be built using them [18]. A qubit is a two level state that also accepts linear combination in its description. Therefore, a qubit can be represented as,

$$|\psi\rangle = \alpha\,|0\rangle + \beta\,|1\rangle\,, \tag{2.1}$$

where α and β are complex numbers that hold the normalization property $|\alpha|^2 + |\beta|^2 = 1$. Also, $|0\rangle$ and $|1\rangle$ are the computation basis. The state vector can be represented in the matrix form,

$$|0\rangle = \begin{bmatrix} 1 \\ 0 \end{bmatrix} \quad |1\rangle = \begin{bmatrix} 0 \\ 1 \end{bmatrix}.$$

Hence, Equation (2.1) is a two dimensional vector in a complex state. The states where $|\beta|^2 = 0$ or $|\alpha|^2 = 0$, that is, $|0\rangle$ and $|1\rangle$. Since the measurements are classical, one can only obtain $|0\rangle$ or $|1\rangle$ in this representation when measuring a qubit. The eigenvalues related to the eigenstates $|0\rangle$ and $|1\rangle$ are 1 and -1, respectively. For example, when a qubit is in the following superposition state,

$$|\psi\rangle = \frac{1}{\sqrt{2}}\,|0\rangle + \frac{1}{\sqrt{2}}\,|1\rangle\,, \tag{2.2}$$

the probabilities are measuring $|0\rangle$ with 50% and $|1\rangle$ with 50%. Although one can argue that infinite information can be stored in one qubit, it is necessary to remember that the outcome of a measurement is either 1 or -1. This also means that, the measurement changes the state of the qubit. It can go from a superposition state to a specific state.

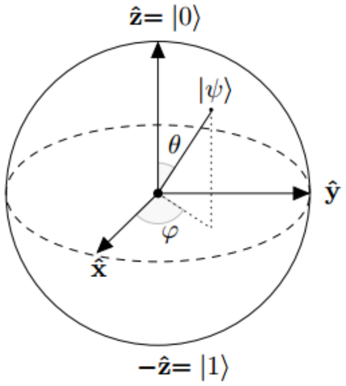

Figure 2.1: Illustration of a qubit in the Bloch sphere.

A very important description form of a qubit is its geometrical representation. In this description, $|\psi\rangle$ can be written as

$$|\psi\rangle = \cos\left(\theta/2\right)|0\rangle + e^{i\phi}\sin\left(\theta/2\right)|1\rangle \tag{2.3}$$

where θ and ϕ are the angles of spherical coordinates. We know that a state, such as in Equation (2.1), has the normalization rule $|\alpha|^2 + |\beta|^2 = 1$, which can be related to the trigonometrical identity $\sin^2\theta + \cos^2\theta = 1$; therefore, the coefficients in Equation (2.3).

Further, the global phase makes no difference, so we can chose either α or β to be real. This description, given θ and ϕ, gives us a defined point in a three dimension sphere, called the Bloch sphere, illustrated in figure 2.1. This sphere is of unit radius so, in each point of its surface lies a pure state. Opposite points represent a pair of mutually orthogonal states. In addition, $|0\rangle(\theta = 0)$ is the north pole and $|1\rangle(\theta = \pi)$ is the south pole. It is worth mentioning that this description is limited since there is no generalization for multiple qubits.

Density Matrix

Another formulation is viable. It is done by using a tool called the *density operator* or *density matrix*. In the state vector formulation, we assume that the state is perfectly determined, which is not always true. So whenever we are in that case, the information we hold is incomplete. What is known is that, provided all available states in the system $\{|\psi_1\rangle, |\psi_2\rangle, ..., |\psi_n\rangle\}$, the target state is in an ensemble of all these available states. In this ensemble, the states are not necessarily orthogonal and each of them has the probability given by $\{p_1, p_2, ..., p_n\}$, correspondingly. These probabilities satisfy the condition $\sum_n p_n = 1$. When in this configuration, we have a *mixed-state* that can be also called a *statistical mixture*. Every single state $|\psi_k\rangle$ in the ensemble is a *pure-state*. Although we cannot express a mixed-state as a state vector, it is possible to describe it in the density matrix formulation. It is defined as,

$$\rho = \sum_k p_k |\psi_k\rangle \langle\psi_k| . \tag{2.4}$$

The operator ρ is called the density matrix because it has a matrix representation. Given a basis in a n-dimension Hilbert space $\{|i\rangle\}$, with $i = 1, 2, ...n.$, the density matrix elements are defined as

$$\rho_{ij} = \langle i| \rho |j\rangle . \tag{2.5}$$

Now it will be introduced a few properties that can be defined using this operator. The mean value of an operator A is,

$$\langle A\rangle = \sum_n p_n \langle\psi_n| A |\psi_n\rangle . \tag{2.6}$$

The trace of an operator is the sum of its diagonal elements in a orthonormal basis $\{|\psi_i\rangle\}$, thus,

$$\mathrm{Tr}(A) = \sum_i \langle\psi_i| A |\psi_i\rangle . \tag{2.7}$$

In the density matrix formalism, the mean value of A can be expressed in a different form. Hence, with the definition we saw in Equation (2.4), we have

$$\begin{aligned} \mathrm{Tr}(\rho A) &= \sum_i \langle\psi_i|\, \rho A \,|\psi_i\rangle \\ &= \sum_k p_k \langle\psi_k|\, A \,|\psi_k\rangle = \langle A\rangle. \end{aligned} \tag{2.8}$$

Then, from Equation (2.8) we can get a few properties of the trace operation. First, we can see that it does not depend on the basis $\{|\psi_i\rangle\}$ to calculate the mean value of the operator A. Second, if we choose $A = \mathbb{1}$ we get,

$$\mathrm{Tr}(\rho) = \sum_k p_k = 1 \tag{2.9}$$

which is the reflection that the sum of a complete set of probabilities is unity. This relation is also connected to the normalization condition where $\langle\psi|\psi\rangle = 1$. Moreover, when writing ρ in its eigenvector basis, $\rho = \sum_k \rho_k |\psi_k\rangle\langle\psi_k|$, we find that

$$\mathrm{Tr}(\rho) = \sum_k \rho_k = 1. \tag{2.10}$$

Therefore, the sum of density matrix eigenvalues is one. The evolution of the density operator is given by Schrödinger equation. Defining $\rho_0 = \sum_k p_k |\psi_k(t=0)\rangle\langle\psi_k(t=0)|$, it is possible to determine ρ's evolution. The quantum states can be written as,

$$\begin{aligned} |\psi_k(t)\rangle &= U(t)\,|\psi_k(t=0)\rangle \\ \langle\psi_k(t)| &= \langle\psi_k(t=0)|\, U^\dagger(t), \end{aligned}$$

where $U(t)$ is any unitary operator and we can assume that it is the temporal propagator,

$$U(t) = e^{-i\mathcal{H}t/\hbar}. \tag{2.11}$$

This expression is valid only for time-independent Hamiltonians. So the density matrix evolution is,

$$\begin{aligned} \rho(t) &= \sum_k p_k U(t)\,|\psi_k(t=0)\rangle\langle\psi_k(t=0)|\, U^\dagger(t) \\ &= U(t)\left(\sum_k p_k |\psi_k(t=0)\rangle\langle\psi_k(t=0)|\right) U^\dagger(t) \\ &= U(t)\rho_0 U^\dagger(t). \end{aligned} \tag{2.12}$$

This formulation also has a geometrical representation. In the sphere's surface lies a pure state, consequently, it can be written as in Equation (2.3). The corresponding density operator is,

$$\rho(\theta,\phi) = \left|\psi(\theta,\phi)\right\rangle \left\langle\psi(\theta,\phi)\right|, \tag{2.13}$$

and its matrix representation in the $\{|0\rangle, |1\rangle\}$ basis is,

$$\rho(\theta,\phi) = \begin{pmatrix} \cos^2(\theta/2) & \sin(\theta/2)\cos(\theta/2)e^{-i\phi} \\ \sin(\theta/2)\cos(\theta/2)e^{i\phi} & \sin^2(\theta/2) \end{pmatrix}.$$

Later in this dissertation it will be discussed the use of spins as qubits.

2.1.2 Quantum Gates

A single bit in classical computation has only one non-trivial logical gate, the NOT gate. It is defined by its true table,

$$\begin{aligned} 0 &\longrightarrow 1 \\ 1 &\longrightarrow 0. \end{aligned} \tag{2.14}$$

For quantum bits, the theory is more complex. We can define an operator X, corresponding to the NOT gate, that interchanges the states ($\alpha|0\rangle + \beta|1\rangle \longrightarrow \alpha|1\rangle + \beta|0\rangle$). This is possible due to the unitary behavior of quantum mechanics. So the quantum NOT gate, X, acts linearly and can be represented in the matrix form as follows,

$$X = \begin{bmatrix} 0 & 1 \\ 1 & 0 \end{bmatrix}.$$

Therefore, X acting on a quantum state gives us,

$$X \begin{bmatrix} \alpha_0 \\ \alpha_1 \end{bmatrix} = \begin{bmatrix} \alpha_1 \\ \alpha_0 \end{bmatrix},$$

provided that the normalization condition must hold before and after the gate action. So the single qubit quantum gates are 2×2 matrices and their only requirement is being unitary, therefore,

$$XX^\dagger = X^\dagger X = \mathbb{1}.$$

Another two non-trivial single quantum gates are the Z gate and the H (Hadamard) gate. The Z gate changes the $|1\rangle$ state phase by π and does not change $|0\rangle$. H turns $|0\rangle$ and

$|1\rangle$ into an uniform superposition. In the matrix form we have,

$$Z = \begin{bmatrix} 1 & 0 \\ 0 & -1 \end{bmatrix}.$$

and

$$H = \begin{bmatrix} 1 & 1 \\ 1 & -1 \end{bmatrix}.$$

Considering the Bloch sphere picture, we can interpret these gates as rotations in the sphere. The Hadamard gate is a $\pi/2$ rotation along the y-axis followed by a π rotation along the x-axis. In fact, an arbitrary single-qubit unitary gate can be constructed as a product of rotations,

$$U = e^{i\gamma} \begin{bmatrix} e^{-i\alpha/2} & 0 \\ 0 & e^{i\alpha/2} \end{bmatrix} \begin{bmatrix} \cos(\beta/2) & -\sin(\beta/2) \\ \sin(\beta/2) & \cos(\beta/2) \end{bmatrix}.$$

where γ, α and β are real numbers. This decomposition into rotations is what makes Quantum Information via NMR possible.

2.1.3 Quantum Simulations

Classical computers are not efficient in the matter of quantum simulations. This is due to the exponential growth of Hilbert space as the number of the particles in the system increases. A system with n particles with two degrees of freedom, which is the system we were working with, has 2^n dimension. Since this scales exponentially, simulating quantum evolution becomes impractical for a large number of particles.

A quantum state evolution is described as follows,

$$|\psi(t)\rangle = e^{-i\mathcal{H}t/\hbar} |\psi(t=0)\rangle \tag{2.15}$$

where $\mathcal{H}$ is the system's Hamiltonian and it is time independent. So the problem is to go from a continuous system to a discrete system, therefore, the discretization of the Hamiltonian is necessary. For this, one can use a set of unitary and discrete operations $U_k(\Delta t_k)$, which is equivalent to the time evolution operator. As a result, the temporal evolution is described as,

$$e^{-i\mathcal{H}_s t/\hbar} = \prod_k U_k(\Delta t_k), \tag{2.16}$$

where $\mathcal{H}_s$ is the Hamiltonian we wish to simulate. Also, $\sum_k \Delta t_k = t$ where t is the simulation total time. Simulating $\mathcal{H}_s$ can be not only very difficult but also produce unsatisfactory results. The first order approximation is given by,

$$e^{-i\mathcal{H}_s t/\hbar} \approx \mathbb{1} - i\mathcal{H}_s t/\hbar. \tag{2.17}$$

Now focusing in the Hamiltonian, if the system's Hamiltonian can be divided into two parts, $\mathcal{H}_s = \mathcal{H}_0 + \mathcal{H}_1$, where $\mathcal{H}_0$ acts like the main Hamiltonian and the second as a perturbation, we can use another approximation. Hence, it can be written as,

$$\mathcal{H} = \sum_k \mathcal{H}_k. \tag{2.18}$$

In general, $[\mathcal{H}_k, \mathcal{H}_l] \neq 0$, as a result,

$$e^{-i\mathcal{H}t/\hbar} \neq \prod_k e^{-i\mathcal{H}_s t/\hbar}. \tag{2.19}$$

This problem can be solved by using the so-called Trotter's approximation formula for Hermitian operators,

$$\lim_{n\to\infty} \left[e^{(iAt/n)} e^{(iBt/n)}\right]^n = e^{(i[A+B]t)}. \tag{2.20}$$

This approximation was used in all simulations made in this work. This is because, in all the Hamiltonians we wanted to simulated, their parts did not commute with one another.

2.1.4 Comparing Quantum States

In classical computation, being able to compare strings of bits is essential for several things, such as, noise and signal comprehension analysis. These measurements for comparison in classical information theory were brought to quantum information theory in order to compare two quantum states. The two most common comparison tools for quantum computation are called *fidelity* and *trace distance*. In this work, however, we only used fidelity measurements. Trace distance, as the name implies, has more of a geometrical view, since it gives us the distance between two quantum states. Fidelity, unlike the trace distance, is a measurement of the difference between two quantum states. Let's say a density operator ρ is to be compared with the pure state $|\psi\rangle$. Because this pure state can be written as a density matrix, using the definition we saw in 2.4 (therefore, $|\psi\rangle\langle\psi|$), the comparison between these two is possible. Fidelity measurement can be deduced in a number of different ways. Using the von Neumann projectors [19],

$$\begin{aligned} P_\psi &= |\psi\rangle\langle\psi| \\ P_{\bar{\psi}} &= \mathbb{1} - |\psi\rangle\langle\psi| \end{aligned} \tag{2.21}$$

and the trace operation, we have,

$$\mathrm{Tr}\left(\rho P_\psi\right) = \sum_i \langle\psi_i|\left(\rho|\psi\rangle\langle\psi|\right)|\psi_i\rangle = \langle\psi|\,\rho\,|\psi\rangle = F. \tag{2.22}$$

This equation is also valid for mixed states. The fidelity measurement, given two mixed states ρ_1 and ρ_2, have four properties,

- $0 \leq F \leq 1$;
- $F(\rho_1, \rho_2) = 1$ only if $\rho_1 = \rho_2$;
- It is symmetrical: $F(\rho_1, \rho_2) = F(\rho_2, \rho_1)$;
- It is invariant under unitary transformations of the two states: $F(U\rho_1U^\dagger, U\rho_2U^\dagger) = F(\rho_1, \rho_2)$.

Provided it fulfills the properties above, it can be defined in a number of different ways. In this work, we used it as the main procedure for comparison of experimental data and theoretical previsions.

The way used to calculate it was introduced in [20]. In this calculation method, two density matrices are said orthogonal if the fidelity is equal to zero and if equal to one, they are identical. It is defined as,

$$\mathcal{F} = \frac{\mid \mathrm{Tr}(\rho_1\rho_2) \mid}{\sqrt{\mathrm{Tr}(\rho_1\rho_1^\dagger)\mathrm{Tr}(\rho_2\rho_2^\dagger)}}. \tag{2.23}$$

This was a brief revision of quantum information theory based on what was used to do the theoretical simulations and the experiments.

2.2 An introduction to NMR

Magnetic resonance is a phenomenon found in magnetic systems that possess both magnetic moment and angular momentum. Resonance means that there is a natural frequency in the magnetic systems that can be tuned in [21]. This phenomenon gives us information about the process on the atomic level. Inside a nucleus there are several particles, such as, neutrons and protons. These particle's spins couple together, and thus, they make a total magnetic moment $\boldsymbol{\mu}$ and a total angular momentum $\mathbf{J}$. They are purely quantum, so they can only be described using quantum mechanics and they are responsible for nuclear magnetism. There are several isotopes that have a non-zero angular and nuclear magnetic moments, such as H^1, C^{13}, F^{19}. In NMR experiments, it is mainly used H^1 (proton) for one qubit experiments and the Chloroform, that contains

H^1 and C^{13}, for two qubits experiments. The magnetic moment and the total angular momentum are aligned so, we can write,

$$\boldsymbol{\mu} = \gamma \mathbf{J} \tag{2.24}$$

where γ is called the gyromagnetic ratio. We can define the angular momentum operator introducing a dimensionless operator $\mathbf{I}$. This definition is as follows,

$$\mathbf{J} = \hbar \mathbf{I}. \tag{2.25}$$

Accordingly, $\mathbf{I}^2$ has eigenvalues $I(I+1)$ where I is either integer or half-integer. Also, $\mathbf{I}^2$ commutes with $\mathbf{I}_i$, where i is the **x-y-z** components, that means $\mathbf{I}^2$ and $\mathbf{I}_z$, for example, are well defined when measured together. Then, there exists a set of simultaneous eigenvectors for $\mathbf{I}^2$ and $\mathbf{I}_z$. The $\mathbf{I}_z$ operator has eigenvalues m, where $-I \leq m \leq I$. When we apply an external magnetic field $\mathbf{B}$, the interaction energy this system produces is by the amount of $-\boldsymbol{\mu} \cdot \mathbf{B}$. In NMR systems, the external field is set on the **z**-direction and B_0 is the magnitude of the external magnetic field so, using equations 2.24 and 2.25 we have,

$$\mathcal{H} = -\gamma \hbar B_0 I_z. \tag{2.26}$$

The allowed energies for this Hamiltonian are:

$$E = -\gamma \hbar B_0 m \tag{2.27}$$

and as we are working with I = 1/2, m = -1/2, 1/2, we have two energy levels. In order to detect this form of energy configuration, one must have spectral absorption causing transitions between energy levels, as can be seen in Figure (2.2). To satisfy the conservation of energy, we have,

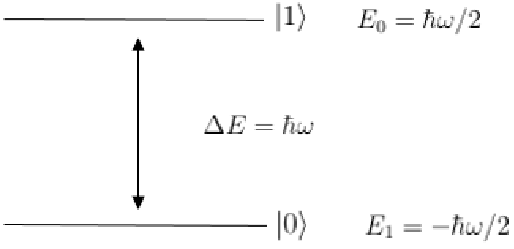

Figure 2.2: Energy split for a 1/2-spin in a magnetic field. The spin gyromagnetic factor is negative; therefore, the ground state is for $m = -1/2$.

$$\hbar\omega = \Delta E \tag{2.28}$$

where ω is the angular frequency and ΔE the difference between the first and the second Zeeman levels. For the purpose of making these transitions viable in a NMR environment, an alternating magnetic field, which is perpendicular to the static magnetic field $\mathbf{H}$, is a necessary choice. The result of this alternating magnetic field is a perturbation in $\mathcal{H}$ in the form,

$$\mathcal{H}_{pert} = -\gamma \hbar H_1 I_x \cos(\omega t) \tag{2.29}$$

where H_1 is the amplitude of the alternating field. I_x has non-zero matrix elements for $m' = m \pm 1$, telling us that transitions between adjacent levels are allowed.

$$\begin{aligned} \hbar\omega = \Delta E &= \hbar \gamma H_0 \\ \therefore \omega &= \gamma H_0. \end{aligned} \tag{2.30}$$

We can see that ω does not depend on $\hbar$ so, it can be closely related to the classical picture. Using a classical approximation, one can find a relation of comparison between $\boldsymbol{\mu}$ and $\mathbf{J}$, and therefore, find that $\gamma = \frac{e}{2mc}$, where e is the particle charge and m its mass. So for nuclear systems immersed in a magnetic field of approximately 10 T,

$$\omega \sim 10\text{MHz}. \tag{2.31}$$

Therefore, ω is in the radio-frequency region.

2.2.1 Spins as Qubits

Quantum particles have, as part of their description, a quantum spin number. The spin dynamics is given by the laws of quantum mechanics. A spin-n particle has $(2n+1)$ degenerate energy levels. If this particle is immersed in an homogeneous magnetic field, this degeneracy is broken. In this work, we used the nuclear spins of ^{13}C and ^{1}H, both having nuclear spin-1/2. Hence, when the degeneracy is broken, they become a two level system. Indeed, any two-level quantum system can provide an implementation of a qubit. Therefore, choosing a spin-half in a magnetic field to be the physical system is a rather convenient choice in the NMR implementation context. In the $\mathbf{I}_z$ operator eigenvector basis the allowed states are $|+1/2\rangle$ and $|-1/2\rangle$, so we can map them as

$$\begin{aligned} |+1/2\rangle &\longrightarrow |0\rangle \\ |-1/2\rangle &\longrightarrow |1\rangle \end{aligned}$$

so the quantum state can be written as,

$$|\psi\rangle = \alpha\,|+1/2\rangle + \beta\,|-1/2\rangle\,. \tag{2.32}$$

Therefore, we have one qubit of information. It is convenient for this spin-half implementation the introduction of Pauli operators.

$$\begin{aligned}\mathbb{1} = &\quad |0\rangle\langle 0| + |1\rangle\langle 1| \\ \sigma_x = &\quad |0\rangle\langle 1| + |1\rangle\langle 0| \\ \sigma_y = &\ i\left(|1\rangle\langle 0| - |0\rangle\langle 1|\right) \\ \sigma_z = &\quad |0\rangle\langle 0| - |1\rangle\langle 1| .\end{aligned}$$

These correspond to the identity operator and the components of the angular momentum in $\hbar/2$ units. Also, they hold the following commutation relation,

$$[\sigma_i, \sigma_j] = 2i\varepsilon_{ijk}\sigma_k \tag{2.33}$$

This commutation property tells us that the Pauli operators have different eigenvectors, this being of the most importance in the NMR implementation of qubits. So, the spin operator is given by,

$$I_i = \frac{\hbar}{2}\sigma_i. \tag{2.34}$$

The association of the spin state can be done in real systems such as in a liquid solution of enriched chloroform, $^{13}CHCl_3$. This system can be approximated by two coupled spins I_1 and I_2 referring to ^{13}C and ^{1}H respectively, thus, two qubits. In this work we used only one qubit implementation, considering only I_2 referred to ^{1}H.

The most basic single bit operations are those that rotate a single spin and can be represented by

$$R_\phi(\theta) = e^{-i\theta\sigma_n/2} \tag{2.35}$$

where θ is the rotation angle and $n = \{x, y\}$. With Equation (2.35) in hands we can convert a quantum evolution into rotations and then implement it experimentally in an NMR equipment.

2.2.2 The Classical Approach

A classical description of a spin in an external magnetic field is the first approach to understand its motion in this given system. The magnetic field $\mathbf{B}$ will produce a torque of the amount $\boldsymbol{\mu} \times \mathbf{B}$. If we were in a frictionless environment, a classical magnetic bar would oscillate around the equilibrium position. Without friction, the oscillations would die and $\boldsymbol{\mu}$ would align with $\mathbf{B}$. If the bar also had angular momentum (in a frictionless environment), it would act like a gyroscope. With friction, the bar would remain fixed in a certain angle but it would precess around it. In a real system, the bearings have friction; therefore, the bar would eventually align with the magnetic field. This is illustrated in figure 2.3. The friction corresponds to the relaxation process called T_1. The equation of motion is, in the laboratory frame, as follows,

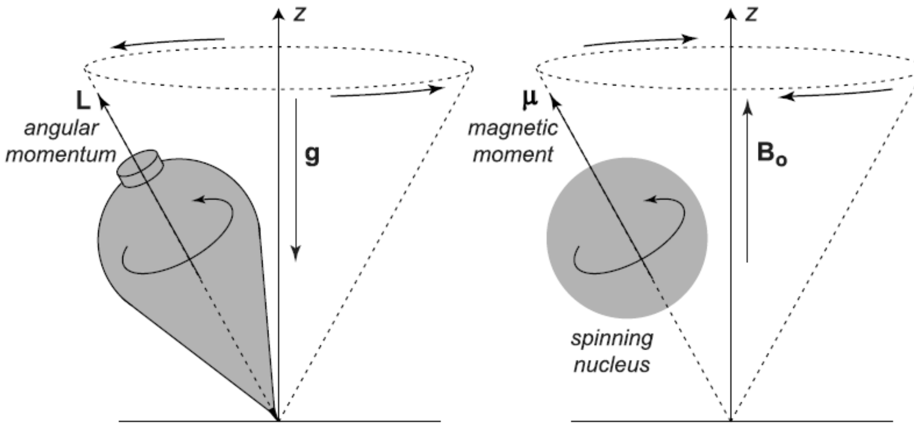

Figure 2.3: Analogy between angular momentum and a spinning nucleus [22].

$$\frac{d\mathbf{J}}{dt} = \boldsymbol{\mu} \times \mathbf{B} \tag{2.36}$$

from 2.24,

$$\frac{d\boldsymbol{\mu}}{dt} = \boldsymbol{\mu} \times (\gamma \mathbf{B})\,. \tag{2.37}$$

As it is described in equation 2.37, the changes in the magnetic moment are always perpendicular to $\boldsymbol{\mu}$ and $\mathbf{B}$. Solving Equation (2.37) can be very complicated. A more useful technique can be used: changing the system's frame into a rotating frame. Considering a vector $\mathbf{F}$,

$$\mathbf{F} = F_x\mathbf{i} + F_y\mathbf{j} + F_z\mathbf{k} \tag{2.38}$$

where $\mathbf{i}$, $\mathbf{j}$ and, $\mathbf{k}$ have fixed lengths but can rotate. Thus,

$$\frac{d\mathbf{F}}{dt} = \frac{\delta \mathbf{F}}{\delta t} + \boldsymbol{\Omega} \times \mathbf{F} \tag{2.39}$$

where Ω is a vector field and $\frac{\delta \mathbf{F}}{\delta t}$ is the time rate of change the coordinate system $\mathbf{i}$, $\mathbf{j}$, $\mathbf{k}$ in time. If it is equal to zero, then $\mathbf{i}$, $\mathbf{j}$ and, $\mathbf{k}$ do not change in time. Now going back to the magnetic moment, we have

$$\frac{d\boldsymbol{\mu}}{dt} = \frac{\delta \boldsymbol{\mu}}{\delta t} + \boldsymbol{\Omega} \times \boldsymbol{\mu} \tag{2.40}$$

as saw in Equation (2.37),

$$\boldsymbol{\mu} \times (\gamma \mathbf{B}) = \frac{\delta \boldsymbol{\mu}}{\delta t} + \boldsymbol{\Omega} \times \boldsymbol{\mu}$$

$$\frac{\delta\boldsymbol{\mu}}{\delta t} = \boldsymbol{\mu} \times (\gamma\mathbf{B} + \boldsymbol{\Omega}) . \tag{2.41}$$

Defining $\mathbf{B}_{eff} = \mathbf{B} + \boldsymbol{\Omega}/\gamma$, Equation (2.41) gets its final form:

$$\frac{\delta\boldsymbol{\mu}}{\delta t} = \boldsymbol{\mu} \times \gamma\mathbf{B}_{eff}. \tag{2.42}$$

It can be seen in this equation that, in the rotating frame, $\boldsymbol{\mu}$ has the same quantitative behavior as in the laboratory frame. Solving 2.42 for $\mathbf{B} = B_0\hat{k}$ and $\boldsymbol{\Omega} = -\gamma B_0\hat{k}$ we have $\frac{\delta\boldsymbol{\mu}}{\delta t} = 0$, which means, $\boldsymbol{\mu}$ is fixed. In the laboratory frame, one would see a fixed vector $\boldsymbol{\mu}$ and the axes rotating with angular velocity $\boldsymbol{\Omega} = -\gamma B_0\hat{k}$ with respect to the laboratory frame or the opposite way around; fixed axes and a vector $\boldsymbol{\mu}$ rotating with a velocity $\boldsymbol{\Omega} = -\gamma B_0\hat{k}$. The quantity γB_0 is called the Larmor frequency. This classical precession frequency $\boldsymbol{\Omega}$ is the same frequency needed for the magnetic resonance absorption.

2.2.3 The Quantum Approach

We know that, in Heisenberg's picture, an operator $\mathbf{F}$ that does not depend explicitly on time can be written as,

$$\frac{d\mathbf{F}}{dt} = \frac{i}{\hbar}[\mathcal{H}, \mathbf{F}]. \tag{2.43}$$

Bringing this to the NMR system, we have the Hamiltonian given by Equation (2.26). The angular momentum operator $\mathbf{I}$ has a cyclic commutation relation,

$$\begin{aligned} [\mathbf{I_x}, \mathbf{I_y}] &= i\mathbf{I_z} \\ [\mathbf{I_z}, \mathbf{I_x}] &= i\mathbf{I_y} \\ [\mathbf{I_y}, \mathbf{I_z}] &= i\mathbf{I_x}. \end{aligned} \tag{2.44}$$

With these relations, one can solve the time variation of each component of $\mathbf{I}$ using equation 2.43 and substituting $\mathbf{F}$ for the angular operator $\mathbf{I}$.

$$\frac{d\mathbf{I_x}}{dt} = \gamma B_0 \mathbf{I_y} \tag{2.45}$$

$$\frac{d\mathbf{I_y}}{dt} = -\gamma B_0 \mathbf{I_x}$$

$$\frac{d\mathbf{I_z}}{dt} = 0, \tag{2.46}$$

which gives us

$$\frac{d\mathbf{I}}{dt} = \mathbf{I} \times \gamma\mathbf{B}. \tag{2.47}$$

The angular momentum and magnetic moment are parallel ($\boldsymbol{\mu} = \gamma\hbar\mathbf{I}$). Hence, we get the same equation of motion for the magnetic moment as in equation 2.42 using properties that are intrinsic to Quantum Mechanics. The only difference is that, in this case, we are dealing with the expected value of the magnetic moment observable. Therefore,

$$\frac{d\left\langle\boldsymbol{\mu}\right\rangle}{dt} = \left\langle\boldsymbol{\mu}\right\rangle \times \gamma\mathbf{B}. \tag{2.48}$$

Thus, equation 2.48 is the same as equation 2.37, which means, the magnetic moment obey classical motion. So far we only considered one spin motion. For a group of spins, their total magnetic moments is

$$\boldsymbol{\mu} = \sum_k \boldsymbol{\mu}_k. \tag{2.49}$$

In the physical system, the sample is dissolved so neither the spin nor the magnetic moments interact with each other. What is measured is the bulk magnetization. Equation 2.48 is also valid for time-dependent magnetic fields.

2.2.4 Bloch Equations

So far, we have only dealt with the magnetic moment. However, what we actually measure in the laboratory is the magnetization. Is it related to $\boldsymbol{\mu}$ in the following form,

$$\mathbf{M} = \frac{\left\langle\boldsymbol{\mu}\right\rangle}{V} \tag{2.50}$$

where V is the sample volume. In the presence of a magnetic field $\mathbf{B}$, there are more magnetic moments aligned with the field than opposite to it. Thus, as a result, the total magnetization is alongside the $\mathbf{B}$ direction. It is worth mentioning that, in the rotating frame, the magnetization has a periodic motion if it is parallel to B_0 and it precesses around it. Remembering that, in the laboratory frame the magnetization is constantly changing its orientation. The system's energy is conserved due to the fact that, what is spent to turn the spins anti parallel is regained when they go back to being parallel to the static field. Hence, we have constant absorption and recovery of energy. The behavior of the total magnetization $\mathbf{M}$ was first described by Felix Bloch in 1946 [23], in a phenomenological approach given by the so-called Bloch Equations.

$$\frac{dM_z}{dt} = \gamma\left(\mathbf{M}\times\mathbf{B}\right)_z - \frac{M_z - M_0}{T_1} \tag{2.51}$$

$$\frac{dM_x}{dt} = \gamma\left(\mathbf{M}\times\mathbf{B}\right)_x - \frac{M_x}{T_2} \tag{2.52}$$

$$\frac{dM_y}{dt} = \gamma\left(\mathbf{M}\times\mathbf{B}\right)_y - \frac{M_y}{T_2} \tag{2.53}$$

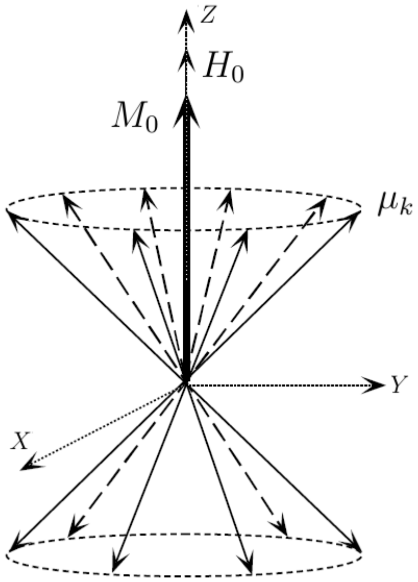

Figure 2.4: Illustration of an thermal state. When immersed in a magnetic field, because it is more energetically favorable, more spins will precess along the magnetic field [22] then against it.

For the longitudinal component, given the magnetization is described in the rotating frame and using an analogy with the population equation[1] we have,

$$\frac{dM_z}{dt} = -\frac{M_z - M_0}{T_1} \tag{2.54}$$

where M_0 is the thermal equilibrium magnetization ($M_0 = \chi_0 B_0$, where χ_0 is the magnetic susceptibility) and T_1 is the longitudinal relaxation time. We know that, in the thermal equilibrium configuration, the magnetization is parallel to the static field. Which means that the **x-y** components of **M** must vanish. Also, we can write the transversal component of the magnetization as such,

$$M_{xy} = M_x + iM_y \tag{2.55}$$

which gives us,

$$\frac{dM_{xy}}{dt} = \gamma \left[(\mathbf{M} \times \mathbf{B})_x + i \left(\mathbf{M} \times \mathbf{B} \right)_y \right] - \frac{M_{xy}}{T_2} \tag{2.56}$$

---

[1] $\frac{dn}{dt} = \frac{n_0 - n}{T_1}$

where T_2 is the transversal relaxation time. Again, in the rotating frame, equation (2.56) can be written as,

$$\frac{dM_{xy}}{dt} = -\frac{M_{xy}}{T_2}. \tag{2.57}$$

One can see that in Equations (2.54) and (2.57) two relaxation times were introduced, T_1 and T_2. T_1 is the longitudinal decay and, it is related to the energy transition time between the thermal reservoir and the system's magnetic moment. T_2 is the transverse decay and it conserves energy in the static field. Therefore, it relaxes without transferring energy to the reservoir. Bloch equations, despite having some limitations, play an important role in the understanding of resonance and relaxation phenomenon. In a typical NMR experiment, the magnetization is observed by studying the *emf* that is induced in the coils of the experimental apparatus.

2.3 Experimental Apparatus

The results of the experiments shown in this work were made in the Nuclear Magnetic Resonance Laboratory in CBPF using a Varian 500 MHz spectrometer. The spectrometer has a cryostat that has two layers of refrigeration, the first uses liquid Helium, and the second liquid Nitrogen. The detection coils stay in the lower part of the equipment and the sample is introduced in the upper part of the cryostat. The sample is at room temperature, which is around 25 degree Celsius. The cryostat contains the superconducting coil, which is responsible for the static magnetic field. This superconductor allows currents of around 10^2 A that generate magnetic fields of the order of 10 T. For the stability and a better homogeneity of the magnetic field, the system is provided with a *shimming* system that corrects these problems. The *shimming* is adjusted by the operator before all the calibration and experiment begins.

The sample used in this work was the enriched chloroform $^{13}CHCl_3$. This molecule is vastly used because of the large resonance frequency difference between ^1H and ^{13}C, this allows one to excite one qubit with minimum noise in the signal due to the interference of the other.

2.3.1 Radio-Frequency Pulses

Consider an isolated spin-1/2 in a strong and homogeneous magnetic field. As we saw, this physical system breaks the degeneracy of the energy levels. Hence, one can manipulate nuclear spins by using an on-resonance RF pulse in the **x-y** plane. These pulses acts like rotations in the states of the nuclear spins. A rotation is described as follows,

$$R_\alpha(\theta) = e^{-i\theta\sigma_\alpha/2} \tag{2.58}$$

where α is the phase and θ is the angle and it has the form $\theta = \omega\Delta t$. Comparing Equation (2.58) with Equation (2.11), one can see that a quantum state evolution can be decomposed into rotations. Also, any rotation in the **x-y** plane can be implemented by a RF pulse given α, θ and the duration time Δt. This is of major importance, because by choosing these corresponding variables, one can interpret a quantum logical gate as a rotation and, therefore, implement it as a series of RF pulses. For example, the **X** gate can be implemented as the following,

$$R_x(\pi) = e^{-i\pi/2}\begin{pmatrix} 0 & 1 \\ 1 & 0 \end{pmatrix}.$$

where $e^{-i\pi/2}$ is a global phase factor, as a consequence, has no effect in unitary transformations. This relation between rotations and quantum gates is, along with many others shown in this work, what makes Quantum Information via NMR possible. A rotation along the z-axis cannot be done by a single RF pulse. One can solve this problem by writing this rotation as a combination of rotations in the **x-y** axes. Therefore,

$$R_z(\theta) = R_x(\pi/2)R_y(\theta)R_x(-\pi/2). \tag{2.59}$$

Another way to implement a rotation around the **z**-axis is to introduce an offset frequency out of resonance. By doing this one shifts the reference frame by an angle θ and all the following pulses will see this as a new reference frame. Consequently, it can be interpreted as rotation by θ around z-axis.

Phase control is of ultimate importance for the correct application of quantum gates with RF pulses. If one implements a π rotation along the **y**-axis we would get,

$$R_y(\pi) = e^{-i\pi/2}\begin{pmatrix} 0 & -1 \\ 1 & 0 \end{pmatrix}.$$

which clearly does not represent the **X** gate. This is due to the sign difference of the matrix elements. Therefore, the control of the phases of the pulses is crucial. RF pulses can produce general spin rotations, consequently, any single qubit gate can be implemented by it.

We wanted to implement and compare a time evolution under three different Hamiltonians. A translation from their theoretical form to the pulse rotation was essential for its development.

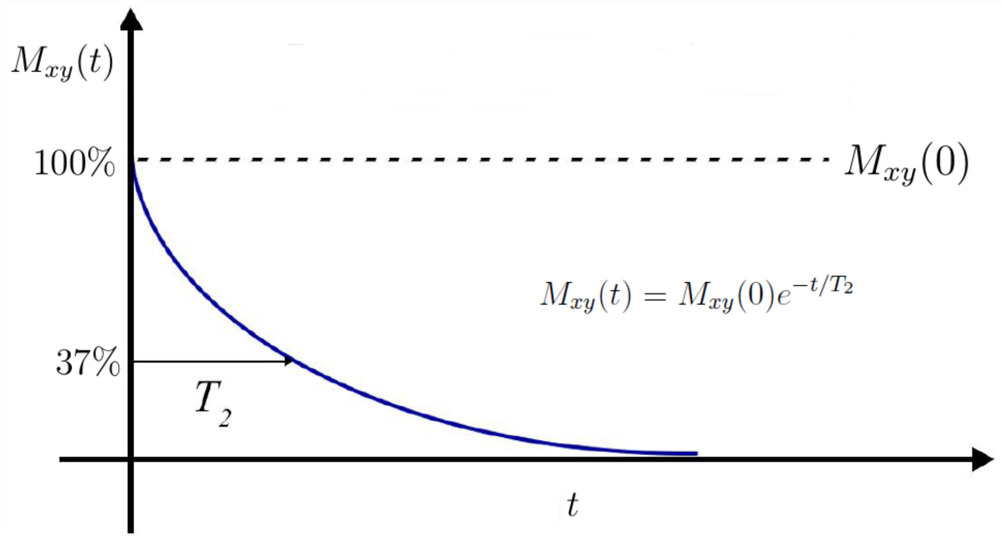

Figure 2.5: The magnetization transversal decay. T_2's value is determined when the magnetization has lost 63% of its value.

2.3.2 Relaxation and Spin Echo

If one applies a $\pi/2$ pulse in a group of spins in order to observe a Free Induction Decay (FID) [24], remembering that all measurements are made in the **x-y** plane, as the pulse is turned off one would see, as described by the Bloch equations, an exponential decay. For liquids, this decay can be of several seconds. It is given by the inhomogeneity of the static field, which makes portions of spins precess a little out of phase from other portions. Since the FID is the sum of all the portions, as the portions get out of phase, the signal decays. The decay time is of the other of $1/\gamma\Delta H$ where ΔH is the spread of the static field. The Bloch equation 2.57, corresponding to the **x-** and **y-** axes combined, gives us a good phenomenological differential equation for the decay.

$$\frac{dM_{xy}}{dt} = -\frac{M_{xy}}{T_2} \tag{2.60}$$

where T_2 is the decay time called *spin-spin* relaxation or transverse relaxation time. The solution to this equation is,

$$M_{xy}(t) = M_{xy}(0)e^{-t/T_2} \tag{2.61}$$

where $M_{xy}(0)$ is the initial transverse magnetization right after the pulse. The transversal magnetization evolution can be seen in Figure 2.5.

Alongside with the transverse magnetization, there is another relaxation process that is physically different from the transverse magnetization. It is called the longitudinal

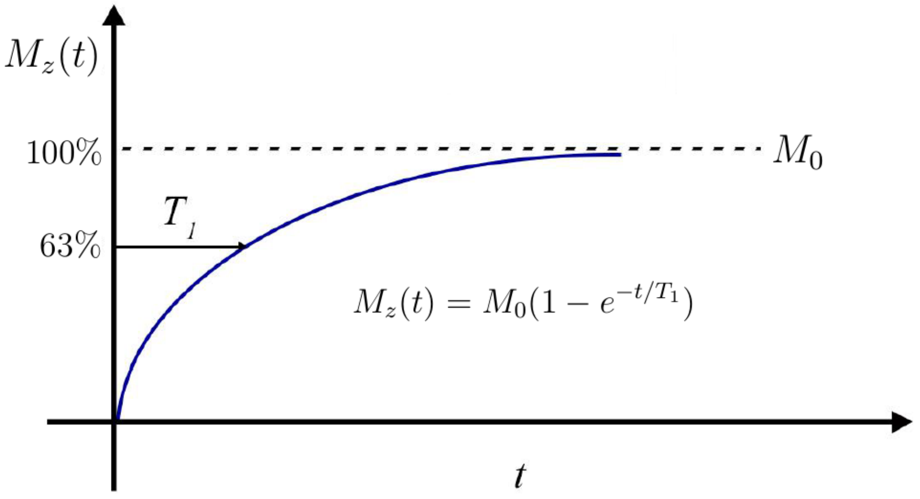

Figure 2.6: The magnetization longitudinal decay. T_1's value is determined when the magnetization has gained 63% of its original value.

magnetization or *spin-lattice* relaxation. This process involves the regain of the thermal equilibrium magnetization. As it was discussed before, there is two energy levels for $m = \pm 1/2$. Whenever $M_z = 0$, these states are equally populated, not corresponding to an equilibrium configuration. The natural tendency would be the system giving up its extra energy to the reservoir, regaining its equilibrium configuration. The environment that gains this extra energy is called lattice; therefore, the *spin-lattice* relaxation. This processes involves, necessarily, exchange of energy and this is the biggest difference from the *spin-spin* relaxation, which involves only the loss of coherence. As for the transverse relaxation, we have the Bloch equation for the z-axis 2.54.

$$\frac{dM_z}{dt} = -\frac{M_0 - M_z}{T_1} \tag{2.62}$$

where M_0 is the initial equilibrium magnetization. T_1 is called the longitudinal or *spin-lattice* relaxation time. The solution can be seen in equation 2.63 and its evolution can be seen on Figure 2.6.

$$M_z(t) = M_0(1 - e^{-t/T_1}) \tag{2.63}$$

This evolution cannot be directly detected since the coils only detect in the **x-y** plane and it is describing the evolution along the **z-** axis. For this reason, if one wants to obtain several measurements, it will be necessary waiting a time bigger than T_1 for the full recovery of the longitudinal magnetization.

Spin echo is the refocusing of the magnetization in the **x-y** plane after a sequence of pulses [25]. It was first discovered by Erwin Hahn in 1950 [26]. An illustration of this phenomenon can be seen in Figure (2.7) The easiest way to understand it is with the $\pi/2 - \pi$ pulse sequence. Consider a group of spins initially in thermal equilibrium in static field $\mathbf{B}$ in the $\mathbf{z}$ direction, M_0 lies parallel to $\mathbf{B}$. For the sake of comparison, lets first neglect the effect of T_1 and T_2. Applying a time dependent magnetic field B_1 at $t = 0$ and $\omega = \gamma B_0$, where ω is the resonance frequency in the y-direction. If there was no inhomogeneity in the static field, all spins would precess with frequency γB_0 and remain orientated along the y'-direction. However, this is not what happens. As a consequence, we must take into account the inhomogeneity of the static field. After a small time τ, since we are not considering the effect of T_1, a portion $\delta\mathbf{M}$ will advance in the $\mathbf{y}$ direction by an angle θ where,

$$\theta = \gamma \delta B \tau \tag{2.64}$$

where δH is the field inhomogeneity. In a time $t = \tau$, we apply a π pulse and after a time $t = 2\tau$, $\delta\mathbf{M}$ will advance again by the same θ but in the opposite direction. Consequently, by the time $t = 2\tau$, all the spins will be in phase again. For times $t > 2\tau$, the dephasing process starts again, being identical when $t = \tau$. Taking T_1 and T_2 into consideration we have that, for $t = \tau$, the $\mathbf{x}$-$\mathbf{y}$ components of $\mathbf{M}$ will decay exponentially with the T_2 action and a $\mathbf{z}$ component will develop exponentially with T_1. After the π pulse, this $\mathbf{z}$ component will be inverted so, it will not contribute to $\delta\mathbf{M}$. During the next τ interval, the decay via T_2 will continue, hence, the magnetization produced by the echo is smaller each time and has the following form,

$$M(2\tau) = M_0 e^{-2\tau/T_2} \tag{2.65}$$

These relaxation phenomena are of the ultimate importance for the implementation of the experiments. Knowing these times is what guarantees not only the minimization of error but also the correct implementation of the quantum gates.

2.4 Quantum State Tomography

Quantum State Tomography (QST) is the characterization of the complete quantum state of a particle given a series of measurements in different bases. In quantum mechanics, we deal with probabilities and mean values, which means, the measurement of a single particle will not give us complete information about the quantum system. As a result, QST must be done in several copies of the same state. This technique can be used to determine any quantum state in any physical system, photons, 2-level atoms and the system we will focus on, spin-1/2 particles.

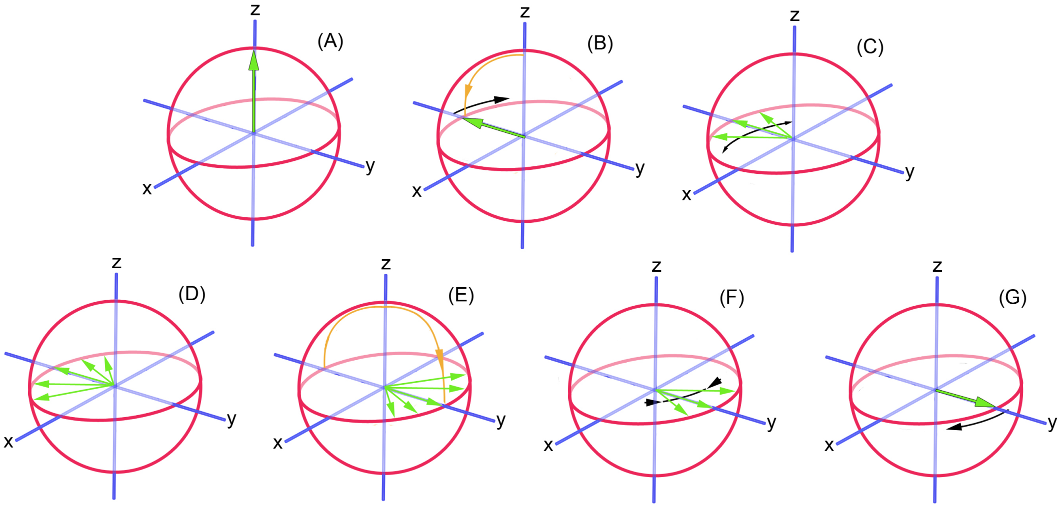

Figure 2.7: Spin echo illustration. We can see that after the $\pi/2$ pulse (B) the loss of decoherence begins (C). Then, a π pulse inverts the magnetization (F) and re refocusing happens.

2.4.1 State Representation

As we saw in the matrix representation of Equation (2.13), a mixed state can be represented by [27],

$$\begin{array}{cc} & \begin{array}{cc} |0\rangle & |1\rangle \end{array} \\ \begin{array}{c} |0\rangle \\ |1\rangle \end{array} & \begin{pmatrix} A^2 & Ce^{-i\phi} \\ Ce^{i\phi} & B^2 \end{pmatrix} \end{array} \tag{2.66}$$

where the coefficients A,B and C are real, non-negative numbers and $A^2 + B^2 = 1$. Another representation for the density matrix is as follows,

$$\rho = \frac{1}{2} \sum_i S_i \sigma_i, \tag{2.67}$$

where $S_0 \equiv 1$ and $i = 0, 1, 2, 3$. This representation uniquely defines a qubit. Hence its density matrix ρ is given by the parameters $\{S_1, S_2, S_3\}$. The connection between Pauli matrices σ_i and the S_i is given by,

$$S_i = \mathrm{Tr}\left(\sigma_i \rho\right). \tag{2.68}$$

For pure states, $\sum_i S_i^2 = 1$ and for mixed states $\sum_i S_i^2 < 1$.

Now it will be described how the exact tomography is done, ignoring all sources of error. For a single-qubit tomography, a sequence of three linearly independent measurements is required. Each measurement corresponds to a degree of freedom. The measurements do not depend on their performance order, the first restrains the state in a plane, the second in a line and the third to a point in the Bloch sphere. Considering S_1, S_2 and S_3 as defined in Equation (2.68), the tomography process is straightforward: measuring in the basis of the eigenvectors of σ_x, σ_y and σ_z is sufficient to complete the tomography. In addition, the state can be measured in any basis.

2.4.2 Quantum State Tomography via NMR

The first part of this chapter was a brief explanation of how (QST) works. Now we move to the experimental approach.

The sample that contains the nuclear spins are usually at room temperature, therefore, the initial system is in a statistical mixture. This initial configuration is unfit for quantum information processing. Spin manipulation provides the creation of pseudo-pure states. Hence, given the initial thermal equilibrium density matrix, the transformations in this system are such that the deviation density matrix is equal to the density matrix of the state wanted. It can be proved that by only doing unitary transformations, one cannot go from a mixed state to a pure state; hence, some non unitary transformations are required. There are several ways of implementing these transformations, for instance, temporal and space averaging and logical labeling. These will not be discussed in this dissertation.

Until now, we only discussed the preparation of initial states and implementing quantum gates. However, the reading out of the results is equally important. This readout, that can be made in different basis, is equivalent to rotating the qubtis and performing the measurement in a fixed basis. With this property, we can rotate the qubits via RF pulses and measure in the I_z basis. The reconstruction of the density matrix is done by the NMR spectra after obtained with the measurement. Hence, one performs a set of unitary rotations via RF pulses to implement the desired evolution. After that, the complete readout is made by applying RF pulses to the final state to reconstruct the final density matrix. As said before, to determine all elements of the final density matrix, it is necessary to perform several measurements. Thus, if the system has only one copy, it cannot be done. However, in NMR this can be done with a single measurement. This is because, in the samples used to perform the experiments, there are several nuclear spins, that is, state copies. So, when performing a single measurement, we can actually get the necessary state statistics. It can be easier to visualize not only the QST but also a quantum evolution using the Bloch sphere approach. In this geometrical approach, the QST is represented by a vector trajectory in the Bloch sphere. For one qubit, the set $\{\mathbb{1}, \sigma_x, \sigma_y, \sigma_z\}$ forms an orthonormal basis where we can expand any operator ρ, as we saw in Equation (2.67). Therefore,

$$\rho = \frac{1}{2}\left[\mathbb{1} + S_1\sigma_x + S_2\sigma_y + S_3\sigma_z\right]. \tag{2.69}$$

where the $S_i's$ are given by Equation (2.68). The mean values of the $\sigma_i's$ are proportional to the magnetization in each **x-y-z** direction. These mean values correspond to the

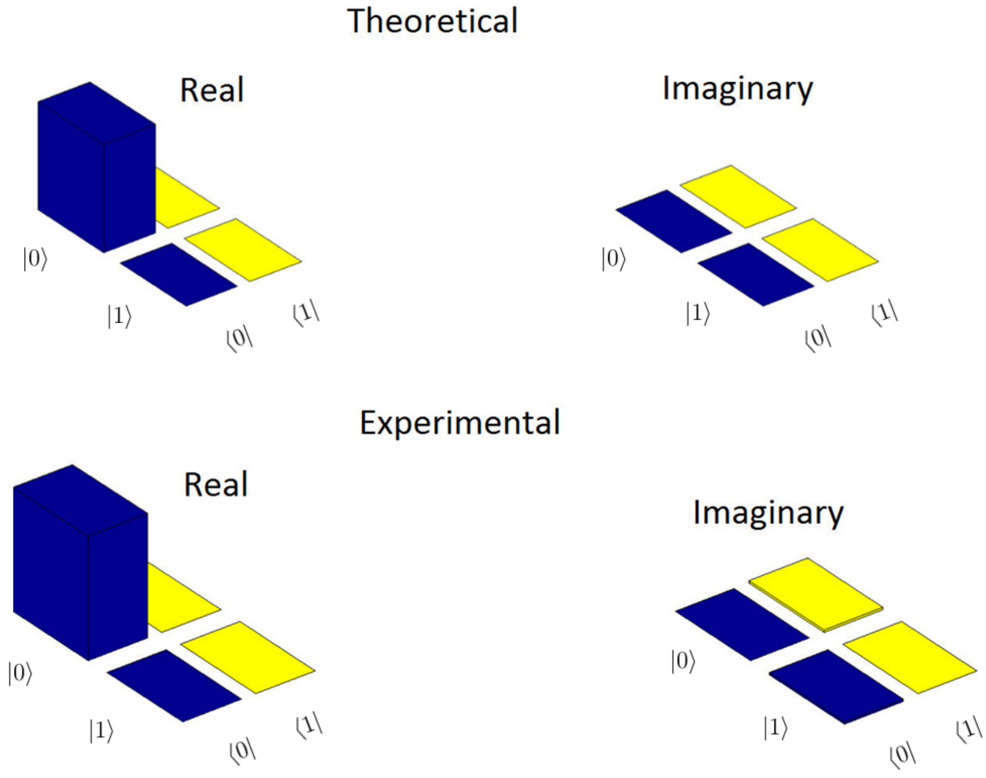

Figure 2.8: Graphical representation of the theoretical density matrix and the reconstructed density matrix via QST. The theoretical state we wanted to measure is $|0\rangle$.

magnetization in the respective direction,

$$\begin{aligned} \mathrm{Tr}(\rho\sigma_x) &= M_x \\ \mathrm{Tr}(\rho\sigma_y) &= M_y \\ \mathrm{Tr}(\rho\sigma_z) &= M_z. \end{aligned} \tag{2.70}$$

However, measurements in NMR are done in the **x-y** plane. This means that the S_1 and S_2 measurements are straightforward, but S_3 is not. To obtain its values, a $\pi/2$ rotation is required. If a rotation around the **y** axis is performed, the value of S_3 will be proportional to $\langle\sigma_x\rangle$. The average over all the measurements has a standard deviation $1/\sqrt{m}$, where m is the number of measurements. Consequently, we can have an arbitrarily precise measurement of the mean value. The reconstruction of the density matrix, for one qubit, is as follow,

$$\rho = \begin{bmatrix} M_z & M_x - iM_y \\ M_x + iM_y & -M_z \end{bmatrix} \tag{2.71}$$

This reconstruction is generally represented by a bar graphic as can be seen in Figure 2.8. This procedure can be generalized for an arbitrary number of qubits. However, we only performed single-qubit measurements, so this generalization is beyond the scope of this dissertation.

Chapter 3

Shortcuts to Adiabaticity

In Classical Mechanics, an adiabatic process does not involve exchange of heat between the system and the environment. In Quantum Mechanics an adiabatic evolution is when the evolved state is in an instantaneous eigenstate of the Hamiltonian that governs the said evolution. Adiabatic evolutions can be used to implement quantum computation as can be seen in the works [28] and [29]. In order to a quantum evolution to be adiabatic, a time constraint is implied. This constraint requires a very slow dynamics, resulting in very long dynamics. This long times are a direct conflict with the coherence times of the given quantum state. However, it was shown that this time constraint is not always a sufficient condition [30], [31]. An example of this will be presented in this dissertation. Therefore, we can interpret adiabatic dynamics as non-transitional evolutions. These non-transitional evolutions were proposed in ([32] and [33]) in order to develop a way to mimic an adiabatic evolution without the time constraint. Moreover, a generalized non-transitional evolution [16] gives us the possibility to control the phases involved in the dynamics. This phase control enables us to build a Hamiltonian that mimics the adiabatic evolution, hence, shortcuts to adiabaticity.

3.1 Adiabatic Theorem

In Quantum Mechanics, a state evolution is given by the Schroedinger's equation,

$$i\hbar\frac{d}{dt}\left|\psi(t)\right\rangle = \mathcal{H}(t)\left|\psi(t)\right\rangle \tag{3.1}$$

and its goal is to find the state dynamics, given an Hamiltonian $\mathcal{H}(t)$. In this work, we focused only on adiabatic evolutions. These evolutions can be interpreted, in such a way that, there is no transition between energy levels. The system is always in its eigenstate. Then, being $|n(t_1)\rangle$ eigenstate of $\mathcal{H}(t_1)$, after a time t the system will be in the corresponding eigenstate $|n(t_2)\rangle$ of $\mathcal{H}(t_2)$. It is worth mentioning that the system's eigenstates are not necessarily the same throughout the evolution. Indeed, the requirement is that no transitions between energy levels occur. For time-dependent Hamiltonians we have the eigenvalue equation as follows [34],

$$\mathcal{H}(t)\left|n(t)\right\rangle = E_n(t)\left|n(t)\right\rangle \tag{3.2}$$

where $\left|n(t)\right\rangle$ are the instantaneous eigenstates and $E_n(t)$ the corresponding energies. If the time change in the Hamiltonian $\mathcal{H}(t)$ is sufficiently slow, then, the evolution will be given always in $\left|n(t)\right\rangle$ apart from phase factors. One can always describe a quantum state $\left|\psi(t)\right\rangle$ in the $\left|n(t)\right\rangle$ basis

$$\left|\psi(t)\right\rangle = \sum_n C_n(t)e^{-i\alpha_n(t)}\left|n(t)\right\rangle \tag{3.3}$$

where $\alpha_n(t)$ is the dynamical phase factor,

$$\alpha_n(t) = \frac{1}{\hbar}\int_{t_0}^{t} E_n(t')dt'. \tag{3.4}$$

We can write Schroedinger's equation in the eigenstate basis substituting equation 3.3 in equation 3.1, obtaining,

$$i\hbar\frac{d}{dt}\left(\sum_n C_n(t)e^{-i\alpha_n(t)}\left|n(t)\right\rangle\right) = \mathcal{H}(t)\left(\sum_n C_n(t)e^{-i\alpha_n(t)}\left|n(t)\right\rangle\right) \tag{3.5}$$

using equation 3.2 we get as a result,

$$\sum_n \dot{C}_n(t)e^{-i\alpha_n(t)}\left|n(t)\right\rangle + \sum_n C_n(t)e^{-i\alpha_n(t)}\left|\dot{n}(t)\right\rangle = 0. \tag{3.6}$$

Being $\left|m(t)\right\rangle$ another instantaneous eigenstate of the Hamiltonian, we can take the inner product with Equation (3.6),

$$\sum_n \dot{C}_n(t)e^{-i\alpha_n(t)}\left\langle m(t)|n(t)\right\rangle + \sum_n C_n(t)e^{-i\alpha_n(t)}\left\langle m(t)|\dot{n}(t)\right\rangle = 0, \tag{3.7}$$

where $\left\langle m(t)|n(t)\right\rangle = \delta_{nm}$ is equal to one only when $m = n$. Then, we get

$$\dot{C}_m(t) = -\sum_n C_n(t)e^{[i\alpha_m(t)-i\alpha_n(t)]}\left\langle m(t)|\dot{n}(t)\right\rangle. \tag{3.8}$$

Taking $n = m$ out of the sum,

$$\dot{C}_m(t) = -C_m(t)\left\langle m(t)|\dot{m}(t)\right\rangle - \sum_{n\neq m} C_n(t)e^{-i(\alpha_n-\alpha_m)}\left\langle m(t)|\dot{n}(t)\right\rangle. \tag{3.9}$$

For the determination of the term $\langle m(t)|\dot{n}(t)\rangle$, we can take the derivative of Equation (3.2),

$$\dot{\mathcal{H}}(t)\,|n(t)\rangle + \mathcal{H}(t)|\dot{n(t)}\rangle = \dot{E}_n\,|n(t)\rangle + E_n\,|\dot{n}(t)\rangle \tag{3.10}$$

taking the inner product again and remembering that $\mathcal{H}(t)$ is hermitian, therefore; $E_m = E_m^\dagger$. Consequently, we have

$$\langle m(t)|\,\dot{\mathcal{H}}(t)\,|n(t)\rangle + E_m\,\langle m(t)|\dot{n}(t)\rangle = E_n\,\langle m(t)|\dot{n}(t)\rangle \tag{3.11}$$

further,

$$\langle m(t)|\dot{n}(t)\rangle = \frac{\langle m(t)|\,\dot{\mathcal{H}}(t)\,|n(t)\rangle}{E_n - E_m} \tag{3.12}$$

for $n \neq m$. Therefore,

$$\dot{C}_m(t) = -C_m(t)\,\langle m(t)|\dot{m}(t)\rangle - \sum_{n\neq m} C_n(t)e^{-i(\alpha_n-\alpha_m)}\frac{\langle m(t)|\,\dot{\mathcal{H}}(t)\,|n(t)\rangle}{E_n - E_m}. \tag{3.13}$$

Now we can apply the adiabatic approximation. We assume that $\dot{\mathcal{H}}$ is very small since the Hamiltonian is varying slowly. Hence, we have the adiabatic condition given by equation 3.14.

$$|\,\langle m(t)|\,\dot{\mathcal{H}}(t)\,|n(t)\rangle\,| \ll \frac{|E_n - E_m|}{\Delta T_{nm}} \tag{3.14}$$

where ΔT_{nm} is the characteristic time for transition between levels n and m. The adiabatic assumption is that there are no transitions, hence, $\Delta T_{nm} \to \infty$ and consequently $|\,\langle m(t)|\,\dot{\mathcal{H}}(t)\,|n(t)\rangle\,| \to 0$. So, in this context,

$$\dot{C}_m = -C_m\,\langle m(t)|\dot{m}(t)\rangle\,. \tag{3.15}$$

Thus, we have a differential equation to solve in order to discover the coefficients which describe a quantum state in the eigenstate basis. Equation (3.15) can be solved with the introduction of Berry's phase. There is a discussion concerning the condition in Equation (3.14). It is not sufficient to ensure an adiabatic process for Hamiltonians that are not real and are oscillating [35], however, this discussion does not concern this work.

3.1.1 Berry's phase

Solving equation 3.15 given the initial condition $C_m(0) = \delta_{nm}$, we have,

$$C_m(t) = C_m(0)e^{-\int_{t_0}^{t} \langle m(t')|\dot{m}(t')\rangle dt'} = e^{i\gamma_m(t)} \tag{3.16}$$

where

$$\gamma_n(t) = i \int_0^t \langle n(t)|\dot{n}(t)\rangle \, dt. \tag{3.17}$$

The quantum state can be written as we saw in Equation (3.3), hence, substituting $C_m(t)$

$$|\psi(t)\rangle = e^{i(\gamma_n(t) - \alpha_n(t))} |n(t)\rangle \tag{3.18}$$

showing us that $|\psi\rangle$ remains in a eigenstate of $\mathcal{H}(t)$. $\gamma_n(t)$ is the geometric phase introduced by M.V. Berry in 1984 [15]. Therefore, the quantum state is as follows,

$$|\psi(t)\rangle = e^{\frac{-i}{\hbar}\int_{t_0}^{t} E_n(t')dt' - \int_{t_0}^{t}\langle n(t)|\dot{n}(t)\rangle dt'} |n(t)\rangle . \tag{3.19}$$

Now, these adiabatic evolution concepts will be applied in order to create an Hamiltonian. It will implement an evolution that mimics the adiabatic evolution without the time constraint.

3.2 Counter-Adiabatic Hamiltonian

Adiabatic evolutions can be implemented given that an adiabatic Hamiltonian $\mathcal{H}_{SA}(t)$ is constructed [28]. This is also true for gate implementation [36], [37]. As we know, because the evolution is adiabatic, its time is bounded by the adiabatic condition in Equation (3.14). However, an adiabatic evolution can be implemented without this time constraint. This imitation is given by the Counter-Adiabatic Hamiltonian [38].

An evolution operator can be built based in the adiabatic state evolution. By doing this, we can implement an evolution for the shortcut with this operator $U(t)$. Its description is as follows,

$$U(t) = \sum_n e^{\frac{-i}{\hbar}\int_{t_0}^{t} E_n(t')dt' - \int_{t_0}^{t}\langle n(t)|\dot{n}(t)\rangle dt'} |n(t)\rangle \langle n(t_0)| . \tag{3.20}$$

Being $|\psi(t_0)\rangle = |n(t_0)\rangle$ the initial state, we can see that this evolution operator actually implements the adiabatic evolution, as is shown in Equation (3.21).

$$U(t)|\psi(t_0)\rangle = \sum_n e^{\frac{-i}{\hbar}\int_{t_0}^{t} E_n(t')dt' - \int_{t_0}^{t}\langle n(t)|\dot{n}(t)\rangle dt'} |n(t)\rangle \langle n(t_0)| |n(t_0)\rangle = |\psi(t)\rangle \tag{3.21}$$

Therefore, $U(t)$ is the adiabatic evolution operator.

The way to implement the shortcut is to add a counter-adiabatic term to the original Hamiltonian that still holds $|\psi(t)\rangle = U(t)|\psi(t_0)\rangle$. Hence,

$$\mathcal{H}_{SA}(t) = \mathcal{H}(t) + \mathcal{H}_{CD}(t) \tag{3.22}$$

where $\mathcal{H}_{SA}(t)$ is the *S*hortcut to *A*diabaticity Hamiltonian. Replacing this new Hamiltonian in Schroedinger's equation, multiplying it by $U^\dagger(t)$ and using the property $U(t)U^\dagger(t) = \mathbb{1}$ we have,

$$U^\dagger(t)\mathcal{H}_{SA}(t)U(t)U^\dagger(t)|\psi_n(t)\rangle = i\hbar U^\dagger(t)|\dot{\psi}_n(t)\rangle \tag{3.23}$$

using the chain rule in the second term,

$$U^\dagger(t)\mathcal{H}_{SA}(t)U(t)U^\dagger(t)|\psi_n(t)\rangle = i\hbar\left[\frac{d}{dt}\Big(U^\dagger(t)|\psi_n(t)\rangle\Big) - \dot{U}^\dagger(t)|\psi_n(t)\rangle\right]. \tag{3.24}$$

Defining $|\psi_m(t)\rangle = U^\dagger(t)|\psi_n(t)\rangle$, we have

$$i\hbar\frac{d}{dt}|\psi_m(t)\rangle = U^\dagger(t)\mathcal{H}_{SA}(t)U(t)|\psi_m(t)\rangle + i\hbar\dot{U}^\dagger(t)|\psi_n(t)\rangle. \tag{3.25}$$

For $t = t_0$,

$$U(t_0) = \sum_n |n(t_0)\rangle\langle n(t_0)| = \mathbb{1} \tag{3.26}$$

hence, $|\psi_m(t_0)\rangle = |\psi_n(t_0)\rangle$. Since the evolution for $|\psi_m(t)\rangle$ is given by $U^\dagger(t)$, it stays always in the eigenstate for $t = 0$. Therefore,

$$\frac{d}{dt}|\psi_m(t)\rangle = \frac{d}{dt}|\psi_m(t_0)\rangle = 0. \tag{3.27}$$

Consequently, the modified Schroedinger's equation becomes, from equation 3.25

$$\Big[U^\dagger(t)\mathcal{H}_{SA}(t)U(t) + i\hbar\dot{U}^\dagger(t)U(t)\Big]|\psi_n(t)\rangle = 0 \tag{3.28}$$

since $|\psi_n\rangle \neq 0$, we have an expression for the adiabatic Hamiltonian. It is given as follows,

$$\mathcal{H}_{SA}(t) = -i\hbar U(t)\dot{U}^\dagger(t). \tag{3.29}$$

Now, we need to determine $\dot{U}^\dagger(t)$. Then,

$$U^\dagger(t) = \sum_n e^{\frac{i}{\hbar}\int_0^t E_n(t')dt' + \int_0^t \langle n(t')|\dot{n}(t')\rangle dt'}|n(t_0)\rangle\langle n(t)| \tag{3.30}$$

accordingly,

$$\begin{aligned}\dot{U}^{\dagger}(t) = &\sum_n \left(\frac{i}{\hbar}E_n(t) + \langle n(t)|\dot{n}(t)\rangle\right) e^{\frac{i}{\hbar}\int_0^t E_n(t')dt' + \int_0^t \langle n(t')|\dot{n}(t')\rangle dt'} \left|n(t_0)\right\rangle \left\langle n(t)\right| \\ &+ \sum_n e^{\frac{i}{\hbar}\int_0^t E_n(t')dt' + \int_0^t \langle n(t')|\dot{n}(t')\rangle dt'} \left|n(t_0)\right\rangle \left\langle \dot{n}(t)\right| . \end{aligned} \tag{3.31}$$

Hence,

$$U(t)\dot{U}^{\dagger}(t) = \sum_n \left(\frac{i}{\hbar}E_n(t) + \langle n(t)|\dot{n}(t)\rangle\right) \left|n(t)\right\rangle \left\langle n(t)\right| + \sum_n \left|n(t)\right\rangle \left\langle \dot{n}(t)\right| \tag{3.32}$$

where $\langle n(t)|\dot{n}(t)\rangle = -\langle \dot{n}(t)|n(t)\rangle$. Now replacing in equation 3.29, we get

$$\mathcal{H}_{SA}(t) = -i\hbar \left[\sum_n \left(\frac{i}{\hbar}E_n(t) + \langle n(t)|\dot{n}(t)\rangle\right) \left|n(t)\right\rangle \left\langle n(t)\right| + \sum_n \left|(n(t)\right\rangle \left\langle \dot{n}(t)\right|\right]. \tag{3.33}$$

Knowing that $\sum_n \left|(n(t)\right\rangle \left\langle \dot{n}(t)\right| = -\sum_n \left|(\dot{n}(t)\right\rangle \left\langle n(t)\right|$, we can finally get the expression for the shortcut,

$$\mathcal{H}_{SA}(t) = \sum_n E_n(t) \left|n(t)\right\rangle \left\langle n(t)\right| + i\hbar \sum_n \left[\langle \dot{n}(t)|n(t)\rangle \left|n(t)\right\rangle \left\langle n(t)\right| + \left|\dot{n}(t)\right\rangle \left\langle n(t)\right|\right]$$

then,

$$\mathcal{H}_{SA}(t) = \mathcal{H}(t) + \mathcal{H}_{CD}(t). \tag{3.34}$$

Therefore, the counter-adiabatic Hamiltonian is given by,

$$\mathcal{H}_{CD}(t) = i\hbar \sum_n \left[\langle \dot{n}(t)|n(t)\rangle \left|n(t)\right\rangle \left\langle n(t)\right| + \left|\dot{n}(t)\right\rangle \left\langle n(t)\right|\right]. \tag{3.35}$$

The $\mathcal{H}_{CD}$ is the Hamiltonian that allows us to mimic the adiabatic evolution. It can be seen that no time constraint is required for its implementation.

3.3 Shortcuts via RMN

Now that the generalized form of the shortcut was introduced, we can manipulate it for the purpose of an application via NMR. The NMR Hamiltonian [30] is as follows,

$$\mathcal{H}_{NMR}(t) = \frac{\hbar\omega_0}{2}\sigma_z + \frac{\hbar\omega_{RF}}{2}\left[\cos(\omega t)\sigma_x + \sin(\omega t)\sigma_y\right] \tag{3.36}$$

where ω_0 is the Larmor frequency, ω_{RF} the strength of the RF field, and ω its frequency. We can calculate its eigenvectors and find the shortcuts for the adiabatic evolution. This

Hamiltonian in the matrix form is given by,

$$\mathcal{H}_{NMR}(t) = \frac{\hbar}{2}\left\{\begin{bmatrix}\omega_0 & 0\\ 0 & -\omega_0\end{bmatrix} + \begin{bmatrix}0 & \omega_{RF}e^{-i\omega t}\\ \omega_{RF}e^{i\omega t} & 0\end{bmatrix}\right\}. \tag{3.37}$$

The eigenvectors for 3.36 are,

$$|n_+(t)\rangle = \cos(\beta/2)\,|0\rangle + e^{i\omega t}\sin(\beta/2)\,|1\rangle \tag{3.38}$$

$$|n_-(t)\rangle = -\sin(\beta/2)\,|0\rangle + e^{i\omega t}\cos(\beta/2)\,|1\rangle \tag{3.39}$$

where $\tan(\beta) = \omega_{RF}/\omega_0$. The experimental values for the ω's will be presented in the next Chapter.

3.3.1 Generalized Non-Transitional Evolutions

In the evolutions governed by Counter-Adiabatic Hamiltonian, the fact that the time constraint is not necessary comes with a disadvantage of higher energy costs for the evolution. Considering a generalized counter-adiabatic theory, we can minimize this energy cost and also find an infinite transition-less model. This is given by the introduction of the arbitrary phase $\theta(t)$. These models include a time-dependent Hamiltonian that implements an evolution with minimal energy cost [16].

For the generalized non-transitional evolutions we can rewrite $U(t)$ as shown in the following equation and then recalculate $\mathcal{H}_{SA}(t)$. Being

$$U(t) = \sum_n e^{i\int_0^t \theta_n(t')dt'}\,|n(t)\rangle\langle n(t_0)| \tag{3.40}$$

where $\theta_n(t)$ are arbitrary real phases. The time evolution is, as expected, $|\psi(t)\rangle = \sum_n e^{i\int_0^t \theta_n(t')dt'}\,|n(t_0)\rangle$. In order to obtain the generalized Hamiltonian, we will proceed in the same way as was done for the counter-adiabatic Hamiltonian. Therefore, recalling that $\mathcal{H}_{SA}(t) = -i\hbar U(t)\dot{U}^\dagger(t)$ we have,

$$\dot{U}^\dagger(t) = -i\sum_n \theta_n(t)e^{-i\int_0^t \theta_n(t')dt'}\,|n(t_0)\rangle\langle n(t)| + \sum_n e^{-i\int_0^t \theta_n(t')dt'}\,|n(t_0)\rangle\langle \dot{n}(t)|. \tag{3.41}$$

Hence, we have the generalized non-transitional Hamiltonian,

$$\mathcal{H}_{SA}(t) = i\hbar\sum_n \left[|\dot{n}(t)\rangle\langle n(t)| + i\theta_n(t)\,|n(t)\rangle\langle n(t)|\right]. \tag{3.42}$$

Since the $\theta_n(t)$'s are arbitrary, one can manipulate them with the purpose of finding ones that can be experimentally implemented.

3.3.2 Optimal Non-Transitional Evolutions

We saw that we can mimic an adiabatic evolution by writing: $\mathcal{H}_{SA}(t) = \mathcal{H}(t) + \mathcal{H}_{CD}(t)$. However, for a number of situations it is not necessary to mimic the exact adiabatic evolution. Making sure that the state remains in an instantaneous eigenstate [39], [40] is sufficient. In this evolution the quantum state is always an eigenstate of the $\mathcal{H}_{NMR}(t)$ Hamiltonian but, its phases are left arbitrary. The phase determination can be done by using the shortcut Hamiltonian and by taking the value of $\theta_n(t)$ that minimizes the energetic cost to execute the dynamics. This gives us the following equation,

$$\theta_n^{op}(t) = -i \langle n(t)|\dot{n}(t)\rangle \tag{3.43}$$

therefore, we get $\mathcal{H}_{SA}^{op}(t)$ by making $\theta_n(t) = \theta_n^{op}(t)$. Using Equations (3.38) and (3.39) in equation 3.42 and $\theta_n^{op}(t)$ we get,

$$\mathcal{H}_{SA}^{op}(t) = \frac{\hbar\omega}{2}\left\{\frac{\sin(2\beta)}{2}\left(e^{-i\omega t}|0\rangle\langle 1| + e^{i\omega t}|1\rangle\langle 0|\right) + (2-\sin^2(\beta))\left(|0\rangle\langle 0| - |1\rangle\langle 1|\right)\right\}. \tag{3.44}$$

Hence, rewriting using the Pauli matrices we have,

$$\mathcal{H}_{SA}^{op}(t) = \frac{\hbar\omega}{2}\left\{(2-\sin^2(\beta))\sigma_z + \frac{\sin(2\beta)}{2}\left(\cos(\omega t)\sigma_x + \sin(\omega t)\sigma_y\right)\right\}. \tag{3.45}$$

Finally, the optimal Hamiltonian is given by,

$$\mathcal{H}_{SA}^{op}(t) = \hbar\left\{\frac{\omega_0^{op}}{2}\sigma_z + \frac{\omega_{RF}^{op}}{2}\left[\cos(\omega t)\sigma_x + \sin(\omega t)\sigma_y\right]\right\} \tag{3.46}$$

where,

$$\omega_0^{op} = \omega(2-\sin(\beta)^2) \tag{3.47}$$

$$\omega_{RF}^{op} = (\omega\sin(2\beta)/2). \tag{3.48}$$

We then, have the Optimal Non-Transitional Hamiltonian.

3.3.3 Adiabatic Phase Non-Transitional Evolutions

For a non-transitional evolution with adiabatic phases, we mimic exactly the adiabatic evolution. This means that, not only the system will always be in an eigenstate of $\mathcal{H}_{NMR}(t)$ but also the phases will be exactly the ones expected in an adiabatic evolution.

Hence, $\theta_n(t) = \theta_n^{ad}(t)$, being

$$\theta_n^{ad}(t) = -\frac{1}{\hbar}E_n(t) + i\left\langle n(t)|\dot{n}(t)\right\rangle \tag{3.49}$$

and with this expression we can obtain $\mathcal{H}_{SA}^{ad}(t)$. However, as we saw in equation 3.34, we can just add the generalized phase Hamiltonian to the $\mathcal{H}_{NMR}(t)$ Hamiltonian in order to obtain $\mathcal{H}_{SA}^{ad}(t)$ in a simpler way. Consequently,

$$\mathcal{H}_{SA}^{ad}(t) = \hbar\left\{\frac{\omega_0^{ad}}{2}\sigma_z + \frac{\omega_{RF}^{ad}}{2}\left[\cos(\omega t)\sigma_x + \sin(\omega t)\sigma_y\right]\right\} \tag{3.50}$$

where

$$\omega_0^{ad} = \omega_0 + \omega(2 - \sin(\beta)^2) \tag{3.51}$$

$$\omega_{RF}^{ad} = \omega_{RF} + (\omega\sin(2\beta)/2). \tag{3.52}$$

3.4 Resonance Condition

The adiabatic condition is not always sufficient to ensure a non-transitional evolution [41]. In systems that present a resonance frequency that can be tuned in, it was shown theoretically in [42] and [43] and experimentally in [31], that when said system is in its resonance frequency the adiabatic condition is violated. Hence, we wanted to implement the shortcuts Hamiltonians in the on-resonance context and see if the adiabaticity would still hold.

To deduce the resonance condition, one can solve the Von Neumann equation. Considering the pure state $\rho(t) = |\psi(t)\rangle\langle\psi(t)|$, we have

$$\dot{\rho}(t) = \frac{1}{i\hbar}\left[\mathcal{H}_{NMR}(t), \rho(t)\right]. \tag{3.53}$$

To solve it one can use the ansatz,

$$\rho(t) = e^{\frac{-i}{\hbar}\frac{\omega t}{2}\sigma_z}\rho_\phi e^{\frac{i}{\hbar}\frac{\omega t}{2}\sigma_z} \tag{3.54}$$

where $\rho_\phi = |\phi(t)\rangle\langle\phi(t)|$. Using Equation (3.54),

$$\dot{\rho}(t) = \frac{-i}{\hbar}\frac{\omega}{2}e^{\frac{-i}{\hbar}\frac{\omega t}{2}\sigma_z}\left[\sigma_z, \rho_\phi(t)\right]\sigma_z e^{\frac{i}{\hbar}\frac{\omega t}{2}\sigma_z} + e^{\frac{-i}{\hbar}\frac{\omega t}{2}\sigma_z}\dot{\rho}_\phi(t)e^{\frac{i}{\hbar}\frac{\omega t}{2}\sigma_z} \tag{3.55}$$

hence,

$$e^{\frac{i}{\hbar}\frac{\omega t}{2}\sigma_z}\dot{\rho}(t)e^{\frac{-i}{\hbar}\frac{\omega t}{2}\sigma_z} = \frac{-i}{\hbar}\left[\frac{\omega}{2}\sigma_z, \rho_\phi(t)\right] + \dot{\rho}_\phi(t). \tag{3.56}$$

For the commutator, we have,

$$[\mathcal{H}_{NMR}(t), \rho(t)] = \mathcal{H}_{NMR}(t) e^{\frac{-i}{\hbar}\frac{\omega t}{2}\sigma_z} \rho_\phi(t) e^{\frac{i}{\hbar}\frac{\omega t}{2}\sigma_z} - e^{\frac{-i}{\hbar}\frac{\omega t}{2}\sigma_z} \rho_\phi(t) e^{\frac{i}{\hbar}\frac{\omega t}{2}\sigma_z} \mathcal{H}_{NMR}(t). \tag{3.57}$$

Therefore,

$$e^{\frac{i}{\hbar}\frac{\omega t}{2}\sigma_z} [\mathcal{H}_{NMR}(t), \rho(t)] e^{\frac{-i}{\hbar}\frac{\omega t}{2}\sigma_z} = \left[e^{\frac{i}{\hbar}\frac{\omega t}{2}\sigma_z} \mathcal{H}_{NMR}(t) e^{\frac{-i}{\hbar}\frac{\omega t}{2}\sigma_z}, \rho_\phi(t) \right]. \tag{3.58}$$

Applying the ansatz to equation 3.53 we can rewrite it as follows,

$$\frac{-i}{\hbar} \left[\frac{\omega}{2}\sigma_z, \rho_\phi(t) \right] + \dot{\rho}_\phi(t) = \frac{-i}{\hbar} \left[e^{\frac{i}{\hbar}\frac{\omega t}{2}\sigma_z} \mathcal{H}_{NMR}(t) e^{\frac{-i}{\hbar}\frac{\omega t}{2}\sigma_z}, \rho_\phi(t) \right] \tag{3.59}$$

and then we get the Von Neumann equation in the new basis,

$$\dot{\rho}_\phi(t) = \frac{1}{i\hbar} \left[\tilde{H}_{NMR}(t), \rho_\phi(t) \right]. \tag{3.60}$$

where

$$\tilde{\mathcal{H}}_{NMR}(t) = e^{\frac{i}{\hbar}\frac{\omega t}{2}\sigma_z} \mathcal{H}_{NMR}(t) e^{\frac{-i}{\hbar}\frac{\omega t}{2}\sigma_z} - \frac{\omega}{2}\sigma_z. \tag{3.61}$$

Finally, $\tilde{\mathcal{H}}_{NMR}(t)$ can be written as,

$$\tilde{\mathcal{H}}_{NMR}(t) = \frac{\omega_0 - \omega}{2}\sigma_z + \frac{\omega_{RF}}{2}\sigma_x \tag{3.62}$$

and in this form one can easily see the resonance condition, $\omega_0 = \omega$.

Finally, we have the NMR Hamiltonian, that is bound to the time constraint shown in equation 3.14 for its evolution to be adiabatic. Using the theory for shortcuts to adiabaticy it was shown that we can remove this time constraint and, thus, have an adiabatic evolution with shorter times. These evolutions are given by $\mathcal{H}_{SA}^{op}(t)$ and $\mathcal{H}_{SA}^{ad}(t)$. The scope of this dissertation is to implement these Hamiltonians experimentally. In addition, verify that the said Hamiltonians mimic an adiabatic evolution even when the adiabatic condition is broken; therefore, when the system is on its on-resonance condition.

Chapter 4

Shortcuts to Adiabaticity via NMR

We saw in Chapter 3 the theory involving adiabatic evolutions. However, performing experiments still remains a real challenge. This is mainly because of the conflict between sufficiently long times necessary for the adiabatic evolution and severely short decoherence times in quantum experiments. The introduction of the shortcuts eliminates this problem and this is what will be verified in this chapter.

It will be explained how the experiment was performed in order to obtain the results that will be shown. The experiments were performed in the Nuclear Magnetic Resonance Laboratory in CBPF using a Varian 500 MHz spectrometer. The spectrometer is composed by a cryostat refrigerated internally by an internal layer of liquid Helium and a more external layer of liquid Nitrogen. At the lower part of the equipment, there is a probe with the detection coils and the sample is inserted in it at the upper part of the equipment. The low temperature is required because of the superconducting coil that generates the static magnetic field. The current in the superconducting coil is around 10^2 A generating a magnetic field of approximately 11.7 T. The illustration of this experimental apparatus can be seen in Figure 4.1.

4.1 Calibration and Relaxation

In a NMR experiment, the calibration is the first and the most important step. This is because it is necessary to obtain parameters like amplitudes and widths (in time) that will characterize the RF pulses. The calibration consists in finding out the times, *pw* and *p1*. These set of parameters obtained during the calibration will ensure that the spin rotations are as precise as possible. These spin rotations are the core of the quantum logical gates and necessary for the implementation on any quantum simulation.

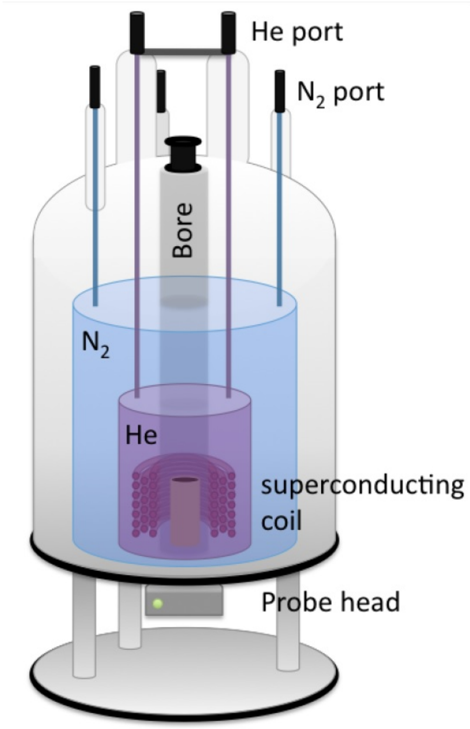

Figure 4.1: Illustration of the NMR spectrometer. The magnet that generates the magnetic field consists in superconducting coils that are refrigerated by the internal layer of liquid Helium.

4.1.1 Sample

The sample used in this experiment was enriched Chloroform ($^{13}CHCl_3$) at room temperature. We used a 5mm probe to measure and positioned with the sample holder so the sample was in a position where the magnetic field is most homogeneous inside the spectrometer. The following step was to adjust its resonance frequency using a built-in function in the system's software called *probe tune*. Using this built-in function we found the following resonance frequency for the Hydrogen:

1H Resonance Frequency
499,861 MHz

4.1.2 Initial Set Up

For Quantum Information experiments it is usually necessary to use the *Lock* function. If the static magnetic field strength changes during the course of the acquisition, the signals will appear broadened and the spectrum will have poor resolution. To keep the field stable, the spectrometer has a mechanism that corrects the field's drift as it occurs; this is the Lock system. The drift is measured using the absorption frequency of the solvent's deuterium resonance (the Lock signal). As this frequency changes due to a change in the field, the system applies an electric current to a coil in the magnet that increases or decreases the field's strength to keep the signal in the same position and the field constant. Once the Lock is set, the next step is to centralize the spectrum so we can tune in the correct resonance frequency. One can either select the PROTON sequence in the software or select the program (written in C language) that implements the same sequence to perform this centralization. This sequence is a solo π pulse, with the purpose of getting a single spectrum. In fact, this acquisition is used not only to verify if the peak is straight enough but also its centralization. When all these procedures are finished, the calibration can begin.

4.1.3 Calibration

The calibration consists in measuring *pw* and *p1* values. These are the values of times, usually in seconds, that the bulk magnetization takes to rotate $\pi/2$ and π around the **x-y** axes, correspondingly. Consequently, the application of a *pw* pulse vanishes the magnetization in the **z** component. In order to find its value, we first apply a π pulse. This operation inverts the magnetization from **z** to **-z** direction. After finding the time it takes for the magnetization to go from one direction to the other, we divide its value by two, therefore, obtaining the *pw* value. The measurements are made in the **x-y** plane, therefore, a π pulse corresponds to a minimum and a $\pi/2$ corresponds to a maximum. It is easier to determine the value of the time where the bulk magnetization is null in the **x-y** plane hence, it is better to use the *p1* measurement and divide it by two to find the *pw* value. To obtain the measurements, one has to use the system's software to make a time array that varies the duration of the pulse. That way the magnetization will, in each pulse, rotate a bigger angle until it finally reaches the final π angle. In each time interval a measurement of the magnetization is performed and with these measurements we can fit a curve and find the values of *pw* and *p1*. Also, we need to wait a time long enough, normally around $90s$, from one measurement to another so that the system will go back to its equilibrium position. All data was processed using MATLAB. The experimental points and the curve that fits these points can be seen in Figure 4.2. The values can be seen in Table 4.1, The determination of *pw* is essential for the pulse manipulation in NMR experiments and also for the longitudinal relaxation time T_1. In the experiment we are implementing, we need to apply pulses that rotate the magnetization by tiny angles so the value of *pw* is crucial not only for the precision but also for the correct implementation of the experiment. After the determination of *pw* and *p1* values, the next step is to measure T_1 and T_2.

	pw	*p1*
1H	$7.63s$	$15,26s$

Table 4.1: Experimental values of *pw* and *p1*.

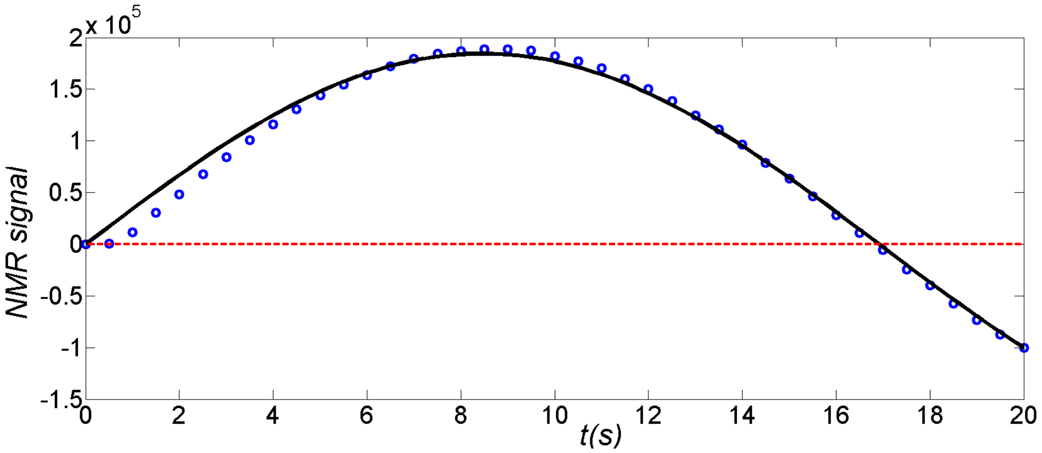

Figure 4.2: Curve that fits the experimental points and gives the experimental value of pw.

4.1.4 T_1 and T_2

Relaxation is related to signal loss as a function of time and its causes are diverse. It is the process of an out of equilibrium state coming back to its equilibrium state. When we quantify these quantities, they can be used in our favour. T_1 (spin-lattice relaxation) is related to the loss of signal intensity, which means, it is the time constant associated with the physical process of magnetization recovery along the **z** direction.

T_2 (spin-spin relaxation) is associated with the coherence loss. That is, the loss of the signal in the **x-y** plane. Due to the fact that the system's equilibrium state depends mainly on the constant applied field H_0, and T_2 is mostly given by spin-spin interactions. The T_1 measurement was made using the inversion recovery process [44] that consists in a π pulse, a time delay, and a $\pi/2$ pulse. The T_2 measurement was made using the CPMG (Carr-Purcell-Meiboom-Gill) process that consists of a $\pi/2$ pulse, a time interval, and π pulses. Both sequences are acquired changing their time interval and for each one of these times a measurement is performed. It is important to emphasize that, in each measurement we need to wait for the system to go back to its equilibrium position to start a new measurement. This time constant is called d_1 and it is usually five times the value of T_1. The values of T_1 and T_2 were acquired by fitting a curve to the experimental results, just like it was done for pw. The curves can be seen in Figures 4.3 and 4.4. The values for T_1, T_2, and d_1 can be seen in Table 4.2.

T_1	T_2	d_1
$5,11s$	$0,25s$	$25s$

Table 4.2: Experimental values of T_1 and T_2 for the Hydrogen isotope.

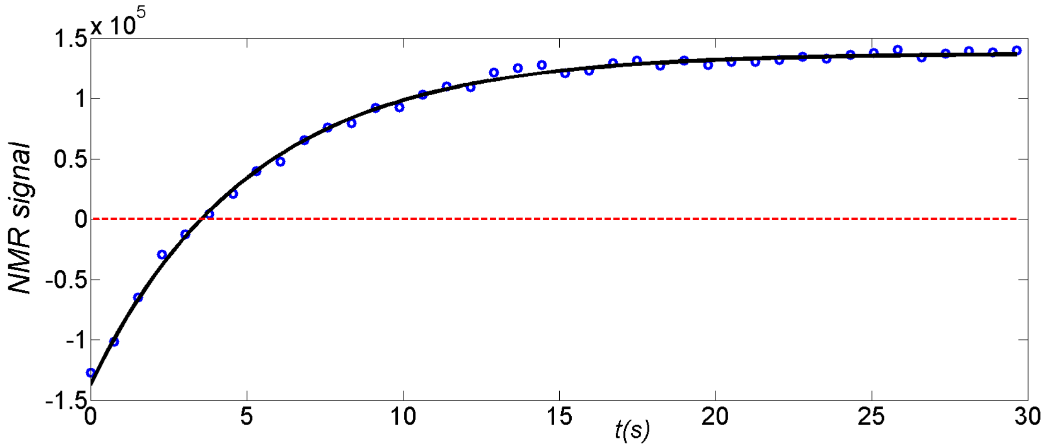

Figure 4.3: Experimental points for the measurement of T_1. One can see that the magnetization starts at a minimum and, as the time interval grows, it stabilizes in the equilibrium magnetization M_0. This graph corresponds to the magnetization on the **z** axis.

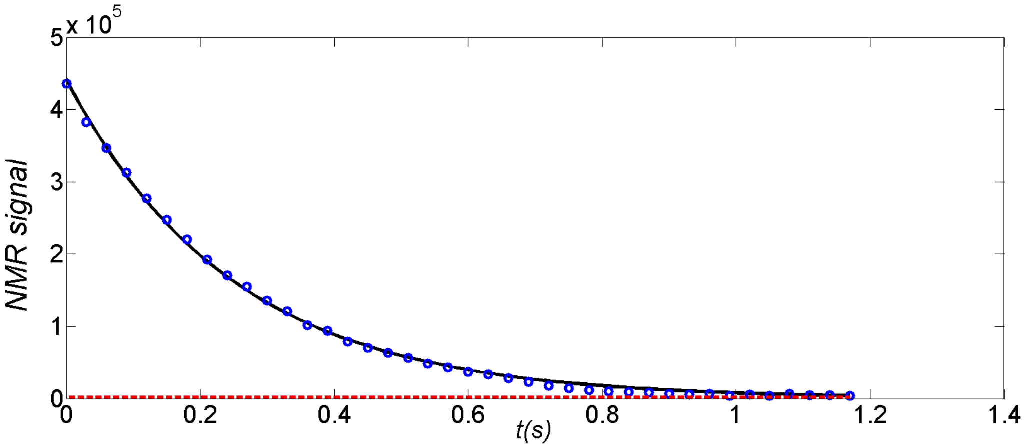

Figure 4.4: Experimental points for the measurement of T_2. One can see that the magnetization starts at a maximum and, as the time interval grows, it goes to zero. This graph corresponds to the magnetization in the **x-y** plane.

4.2 Experimental Implementation

Now we are going through the experimental description that implemented the evolutions governed by the NMR Hamiltonian and the Shortcuts Hamiltonians. In order to verify those evolutions were indeed adiabatic, we calculated the theoretical instantaneous eigenstates for the NMR Hamiltonian for several time intervals Δt. Moreover, we used fidelity as a comparison method comparing the evolved state under each Hamiltonian with the theoretical instantaneous eigenstate for the same interval.

4.2.1 Initial State

We wanted to implement an on-resonance evolution, which can lead to population transfer, resulting in a non-adiabatic evolution. This condition will show that the shortcuts still hold a non-transitional evolution. The eigenstates of the NMR Hamiltonian depend on the values of ω_0, ω_{RF} and ω. We chose the ground eigenstate, which is the following,

$$|n_-(t)\rangle = -\sin\left(\omega_{RF}/2\omega_0\right)|0\rangle + e^{i\omega t}\cos\left(\omega_{RF}/2\omega_0\right)|1\rangle \tag{4.1}$$

and the on-resonance condition dictates that $\omega_0 = \omega_{RF} = \omega$. We numerically calculated the values that gave us the eigenstate.

$$\omega_0 = \omega_{RF} = \omega = 200\text{MHz}. \tag{4.2}$$

These values give the following theoretical initial state,

$$|\psi_{eigen}(t=0)\rangle = \begin{pmatrix} 0,3827 \\ -0,9239 \end{pmatrix} \tag{4.3}$$

and the density matrix,

$$\rho_{eigen} = \begin{pmatrix} 0,1465 & -0,3536 \\ -0,3536 & 0,8536 \end{pmatrix}. \tag{4.4}$$

The theoretical and experimental density matrix can be seen in Figure 4.5. Its fidelity with the theoretical prevision is $\mathcal{F} = 0.9989$.

In NMR systems we are dealing with a statistical mixture of state systems, and in order to get a state that we can work with, we use a sequence of pulses that generate what is called *pseudo pure states.* A quantum state of a system at temperature T can be written as,

$$\rho_{sys} = \frac{e^{-\mathcal{H}_{sys}/k_B T}}{\sum_m e^{-E_m/k_B T}} \tag{4.5}$$

where k_B is the Boltzmann's constant and $\mathcal{H}_{sys}$ is the system's Hamiltonian and its energy levels are given by E_m. It is easy to see that ρ_{sys} is not a pure state, since $Tr(\rho^2) \neq 1$. However, one can extract a pseudo pure state from it by unitary operations. This can be done by transforming the thermal state into the state in equation 4.6.

$$\rho = 2^N\mathbf{I} + \rho_\Delta \mathbf{I}_z \tag{4.6}$$

the first term corresponds to a uniform background, and since it is proportional to the identity operator, it does not evolve in time. The second term, ρ_Δ, called *deviation density matrix*, has a null trace so all unitary evolution acts only in this matrix. The deviation density matrix is proportional to the $\mathbf{I}_z$ operator. N is the total number of spins. In this

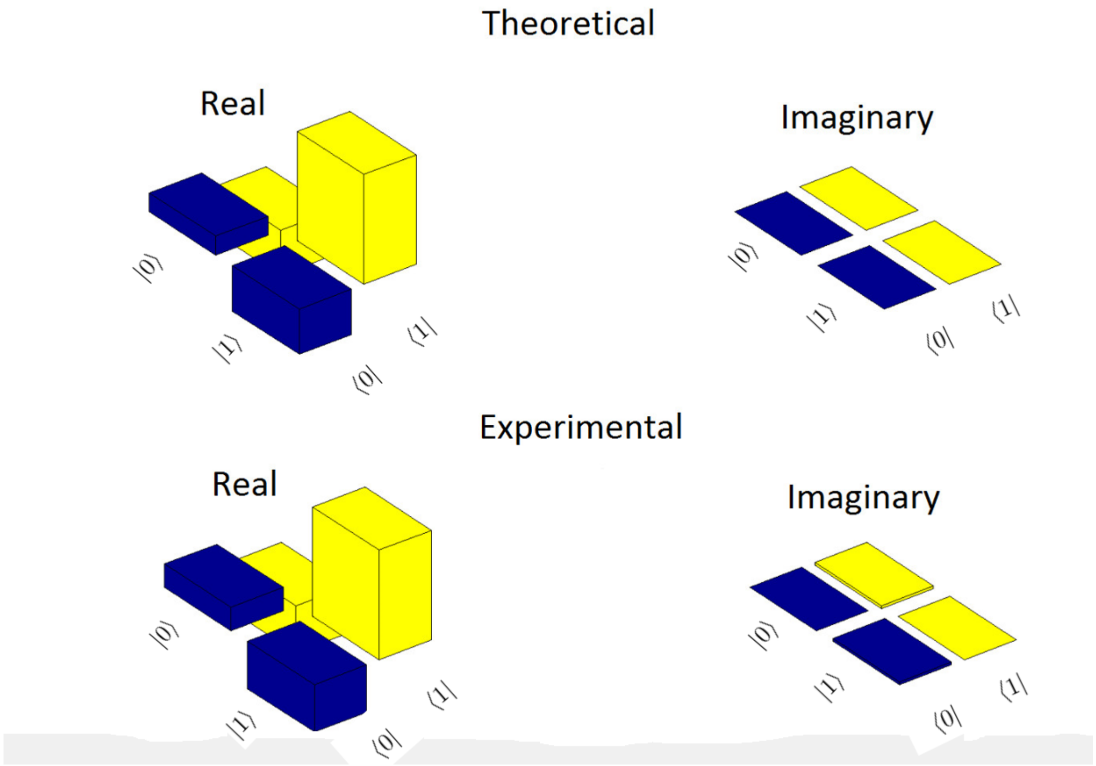

Figure 4.5: Graphical representation of the theoretical density matrix and the reconstructed density matrix via QST. The theoretical state we wanted to measure is $|\psi_{eigen}\rangle$.

system, the pure state after the unitary operations is given by $|0\rangle$. The RF pulse rotates this state, hence we needed to find the correct rotation angle that would implement the initial state given by equation 4.3. The rotation necessary is shown in equation 4.7.

$$R_y(\alpha)\,|0\rangle = |\psi_{eigen}\rangle \tag{4.7}$$

where

$$R_y(\alpha) = e^{-i(\alpha-\pi)\sigma_y/2}. \tag{4.8}$$

The angle found was $\theta = (\alpha - \pi) = -135^{\text{o}}$. Before implementing the pulse sequence that generates $|\psi_{eigen}\rangle$, we need first to measure the $|0\rangle$ state for normalization procedures. This value was also used for the $|\psi_{eigen}\rangle$ normalization.

4.2.2 Shaped Pulses

Shaped pulses can be used for selective excitation [45]. The excitation frequency domain of a RF pulse is the Fourier transform of the time dependent shaped pulse. It determines the width, uniformity and the phase of the excited espectrum. The implementation of the shaped pulses consists in dividing them in several time intervals. With this in mind, one can modulate any shaped pulsed controlling either the pulse's amplitude or its phase. In this work, we implemented the shaped pulses controlling the phase, also called, phase shaping. Moreover, combining multiple shaped pulses applied with different frequencies one can get one simple pulse. This is valid because a linear sum of pulse slices is a valid pulse itself.

The phase shaping method [46] implemented, used fixed small increments $\Delta\phi$ that divided the pulses into slices. These slices have a time duration Δt and these intervals had to be small enough in order to apply Trotter's formula seen in equation 2.20. Based on the problem's parameters, we build a table with the corresponding fixed amplitude, $\Delta\phi$ and Δt. The table provides a file with the respective modulations we want to implement. This file is taken to the computer that controls the spectrometer and with it the pulses are shaped and applied. With these files we generated the theoretical simulation of the evolution, that can be seen in Figure 4.6. We used fidelity, as was defined in equation 2.23, for comparing the instantaneous eigenstates $|n(t)\rangle$ of $\mathcal{H}_{NMR}(t)$ with the evolved states for all three Hamiltonians in the same time interval. As expected, if the evolution is adiabatic, the states will always be given by the instantaneous eigenstates $|n(t)\rangle$ of $\mathcal{H}_{NMR}(t)$, therefore; the fidelity would by equal to 1 throughout the evolution. If the evolution is not adiabatic, then the values of the fidelity would vary during it. The simulation shown in Figure 4.6 was done disregarding decoherence effects.

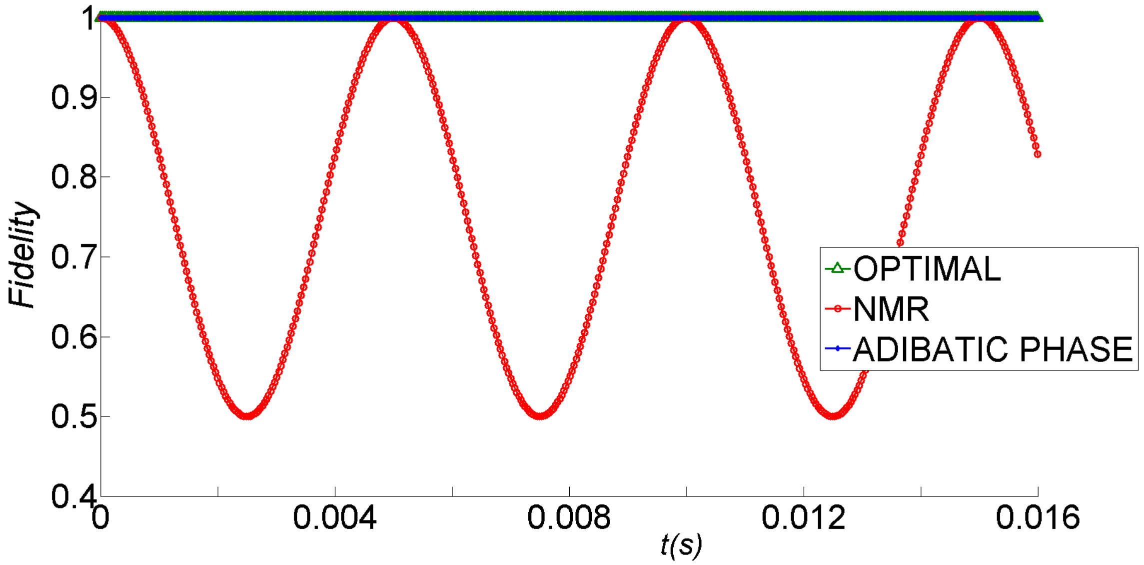

Figure 4.6: Theoretical simulation for evolution of the Hamiltonians $\mathcal{H}_{NMR}(t)$, $\mathcal{H}_{SA}^{op}(t)$ and $\mathcal{H}_{SA}^{ad}(t)$. As we can see, the shortcuts still hold an adiabatic evolution even in the on-resonance condition. Meanwhile, the NMR Hamiltonian does not implement an adiabatic evolution even for long times.

4.2.3 Implementation

To implement Hamiltonians $\mathcal{H}^{op}_{NMR}(t)$, $\mathcal{H}^{ad}_{SA}(t)$, $\mathcal{H}^{op}_{SA}(t)$ we used the shaped pulses technique.

The Hamiltonians have two separate terms, one is time independent (the terms proportional to ω_0). The other (the terms proportional to ω_{RF}) are time dependent. In the spectrometer, we centralized the spectrum in order to put the system in its resonance condition. Since the first term can be interpreted as an *offset* out of the resonance frequency, after this centralization we moved the spectrum out of the resonance frequency by ω_0. We performed this same procedure for all three Hamiltonians with their respective ω_0 values. The values are the following,

$$\begin{aligned}\omega_0 &= 200\text{MHz}\\ \omega_0^{op} &= 300\text{MHz}\\ \omega_0^{ad} &= 500\text{MHz}.\end{aligned}$$

The values of the ω_{RF}'s can be adjusted by finding the RF power that implements them. They are given by,

$$\begin{aligned}\omega_{RF} &= 200\text{MHz}\\ \omega_{RF}^{op} &= 100\text{MHz}\\ \omega_{RF}^{ad} &= 300\text{MHz}.\end{aligned}$$

In order to do so, for each value of ω_{RF} we wanted, we found the time τ that resulted in a spin rotation by 2π. This time was calculated using equation,

$$2\pi f = \omega, \tag{4.9}$$

where $\omega\tau = \theta$. As was said, we want $\theta = 2\pi$, hence

$$\begin{aligned}\omega\tau &= \theta = 2\pi\\ \tau_{2\pi} &= \frac{1}{\omega_{RF}}.\end{aligned} \tag{4.10}$$

Thus, for the three values of ω_{RF},

$$\begin{aligned}\tau_{2\pi} &= \frac{1}{200Hz} = 5ms\\ \tau_{2\pi}^{op} &= \frac{1}{300Hz} = 3.3ms\\ \tau_{2\pi}^{ad} &= \frac{1}{500Hz} = 2ms.\end{aligned}$$

Now we know that for a time τ the signal has to be zero, so we adjusted the RF field power for no signal in the **x-y** plane, therefore; no spectrum. That way we know that we will be implementing the correct ω_{RF}. The values, which are necessary for the correct simulation, that implemented the RF power, called *pwrf*, are the following,

$$\begin{aligned} pwrf &= 229u.a. \\ pwrf^{op} &= 110u.a. \\ pwrf^{ad} &= 336u.a. \end{aligned}$$

Since the second term has a time dependence in its phases, the pulses necessary to implement it were achieved by using the shaped pulse technique. We numerically created the table necessary to build these pulses using the values described above. The table was constructed as can be seen in Table 4.3. Hence, for each time interval a shaped pulse was generated. The files generated by the program in MATLAB were used in the spectrometer program (C language) in order to convert them into physical pulses given the parameters previously calculated.

A	$\Delta\phi$	Δt
ω_{RF}	ωt	1

Table 4.3: Table constructed for the application of the shortcut Hamiltonians. By dividing the RF pulses into slices, they can be modulated in order to implement the Hamiltonian.

4.2.4 State Comparison

As we saw, for the purpose of making the experimental implementation of the Hamiltonian viable, its discretization was necessary. Now, we needed to compare, for each time interval, whether the evolution was indeed adiabatic. Hence, we performed a QST (Quantum State Tomography) for each Δt. This QST constructs the experimental density matrix. The goal is to obtain the bulk magnetization in each **x-y-z** direction and, with those values, reconstruct the density matrix using equation 2.71. The first measurement is to find the M_z value, however, this measurement is not straightforward. Hence, a $\pi/2$ pulse is applied so the bulk magnetization in the z direction gets to the **x-y** plane and the measurement can be performed. The second measurement is performed straightforwardly in the **x-y** plane. The result of those measurements is a FID, the NMR signal. It is the signal generated when the bulk magnetization is non-zero in the **x-y** plane. This magnetization, that is always precessing (as we saw in Figure 2.3), will generate a proportional oscillating voltage in the detection coils that surround the sample [47]. After the Fourier transform of the NMR signal (**FID**) we get [48],

$$S^1(t) \propto \left\{ tr(\rho\sigma_x) + itr(\rho\sigma_y)e^{i\omega t} \right\}. \tag{4.11}$$

where the index 1 stands for one qubit signal. Therefore, for the values of M_x and M_y we took the Fourier transform of this *FID* and integrated the spectra; the real part corresponds to M_x and the imaginary to M_y. The *FID* for M_z is a linear combination of the x and y components, given as follows

$$S^x(t) \propto \left\{ tr(\rho\sigma_x) - itr(\rho\sigma_z)e^{i\omega t} \right\} \tag{4.12}$$

$$S^y(t) \propto \left\{ tr(\rho\sigma_z) + itr(\rho\sigma_y)e^{y\omega t} \right\}. \tag{4.13}$$

Hence, these unitary transformations convert the expected values of $\langle\sigma_x\rangle$ and $\langle\sigma_y\rangle$ into $\langle\sigma_z\rangle$.

4.3 Analysis

The results of those implementations can be seen in Figure 4.7. As expected, we see that the adiabatic condition does not hold for $\mathcal{H}_{NMR}(t)$ and we can see the shortening of the oscillation amplitudes. This is due to the decoherence effects, given not only the interaction of the quantum states with the environment, but also because the RF pulses have errors of implementation of their own. Those errors are about 3% per pulse. Due to the decoherence effects the amplitudes decrease. The oscillations shows that the NMR Hamiltonian does not implement an adiabatic evolution in the on-resonance condition.

The shortcuts experimental implementation has shown to be very robust against the decoherence process. This can be seen because the fidelity stays close to one throughout the evolution, which means that the states of the evolution are, indeed, instantaneous eigenstates of $\mathcal{H}_{NMR}(t)$. Therefore, one can conclude that the shortcuts are a superior implementation of an adiabatic evolution.

The fitting of the experimental data was performed using Lindblad equation, shown in Equation (4.14), and adjusting its parameters.

$$\dot{\rho} = \frac{i}{i\hbar}\left[\mathcal{H}(t), \rho(t)\right] + \frac{1}{2}\sum_k \left(L_k\rho(t)L_k^\dagger - \frac{1}{2}L_k^\dagger L_k\rho(t) - \frac{1}{2}\rho(t)L_k^\dagger L_k \right) \tag{4.14}$$

where the commutator term is the unitary evolution generator. The second term describes the possible transitions that the system may undergo due to interactions with the thermal reservoir. The operators L_k are called Lindblad operators or quantum jump operators. The term $L_k\rho(t)L_k^\dagger$ is responsible for the possibility of these quantum jumps to happen. The terms $-\frac{1}{2}L_k^\dagger L_k\rho(t) - \frac{1}{2}\rho(t)L_k^\dagger L_k$ that can be rewritten as the anti com-

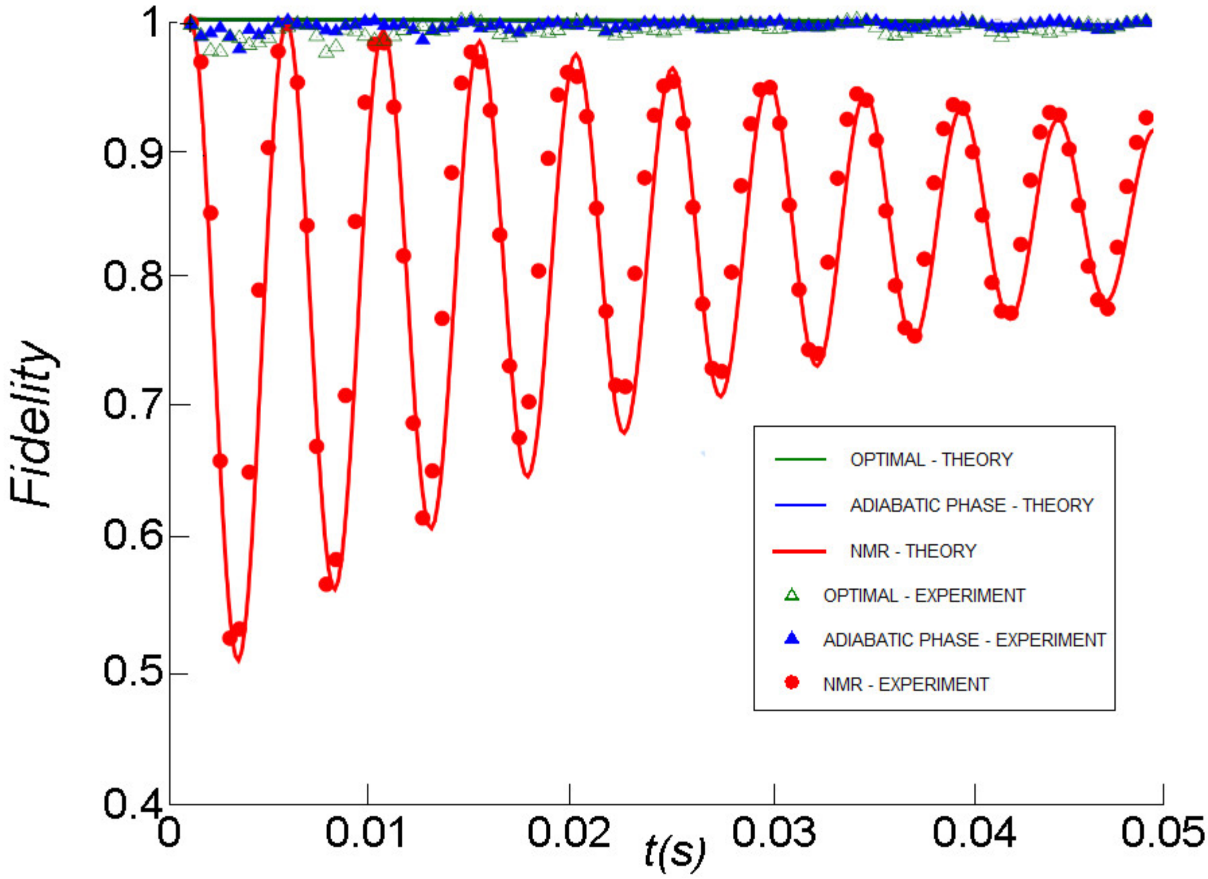

Figure 4.7: Experimental data and theoretical simulations via Lindbald equation. The lines are the theoretical simulation and the points the experimental results.

mutator $-\{L_k^\dagger L_k, \rho(t)\}$. They are needed to normalize in case no jumps occur. It can be shown that for this system, the Lindblad operator is as follows,

$$\Gamma_1(t) = \gamma(t)\sigma_z \tag{4.15}$$

where $\gamma(t) = \sqrt{1/T_2}$. Hence, substituting it in equation 4.14 we have,

$$\dot{\rho} = \frac{i}{i\hbar}\left[\mathcal{H}(t), \rho(t)\right] + \frac{\gamma_0}{2}\left(\sigma_z \rho(t) \sigma_z - \rho(t)\right) \tag{4.16}$$

where $\gamma_0 = \sqrt{1/T_2}$. This was the equation used to calculate the theoretical evolution and with the experimental value of T_2 that was measured, adjust it in the experimental data. Dephasing, or transverse relaxation, is the phenomenon associated with the decay of the coherence terms (off-diagonal) in the density matrix and. As it was discussed in Chapter 2, this occurs due to the inhomogeneity of the static magnetic field. This variation causes the spins of all the molecules to slowly desynchronizes and, therefore, lose coherence across the sample. We only considered the dephasing effect because the evolution time is on the same order of magnitude as T_2 value. The value of T_1 is approximately 10 times bigger than the evolution's total time, so it does not interfere significantly. Therefore, we could adjust the Lindblad equation parameters to explain the experimental results.

This analysis concludes the work wished to be presented in this dissertation.

Chapter 5

Conclusion

In this dissertation we started with a small introduction to Quantum Computation and the motivations why its implementation would be advantageous over Classical Computation. QC is a recently new area in Physics and, therefore, it still has a lot of open problems. Moreover, we defined qubits and how they can be implemented via NMR systems. The advantages of using NMR as a quantum computer and implementing quantum gates and quantum evolution in this system were also discussed. We also talked about how experiments in NMR are performed and the theory regarding it. One can have both classical and quantum approaches to solve the equation of motion for the magnetic moments of nuclear spins. This is very interesting because we see that a purely quantum system can have a classical behaviour. One important characteristic of the NMR technique is that, the relaxation times of the samples generally are a few orders of magnitude bigger than the implementation of the operations itself. This allows the experimental implementation of several RF pulses and, therefore, several quantum gate and/or evolutions without the complete loss of the magnetization signal. It is worth mentioning that, in an NMR experiment is possible to reconstruct the experimental density matrix in a procedure called Quantum State Tomography. This is very useful for analysing the data provided by the experimental implementations.

The adiabatic theorem was first introduced by Boltzmann in Classical Mechanics. Latter its Quantum Mechanics definition was developed. An adiabatic evolution is an evolution that is given always in instantaneous eigenstates of an Hamiltonian. It can be useful for a number of implementations that require the system always evolving in a well-known state. One of the greatest applications of an adiabatic evolution is in Adiabatic Quantum Computation. We also showed that implementing an adiabatic evolution is non trivial and the adiabatic condition is not always sufficient to implement the evolution. Also, that in systems with a natural resonance frequency, when tuned in this frequency, the adiabaticity is broken. We introduced the shortcuts to adiabaticity theory, first considering the counter-adiabatic Hamiltonian and then going one step forward to the generalized non-transition evolution. With it, we could build two Hamiltonians that mimic the adiabatic evolution without the necessity of the adiabatic condition.

The implementation of the shortcut Hamiltonians, alongside with the NMR Hamiltonian, begins with the standard NMR experiment procedure. We talked about the importance of correctly implementing the initial eigenstate since the whole following evolution would depend on it. Further, we introduced the shaped pulse method, and how it was applied to the implementation of the three Hamiltonians. We saw that, indeed, in the on-resonance condition the NMR Hamiltonian does not provide an adiabatic evolution, on the other hand; the shortcuts do. This shows how powerful the general non-transition theory is. We also saw the decoherence acting throughout the experiment and modelled it using the Lindbald equation.

The next step it to implement the quantum phase gate, the **Z** gate, using these Hamiltonians. It will be given by translating the initial Hamiltonians, such as, the state after the evolution is the same state after the application of quantum gate. The Hamiltonians used will be the standard NMR Hamiltonian and the shortcuts Hamiltonian that has the lowest energy cost, thus, $\mathcal{H}_{SA}^{op}(t)$. The goal is to verify, once again, the advantage the shortcut have on the NMR Hamiltonian. What is expected to be verified is that the shortcut Hamiltonian implements the **Z** gate. This means that, for any evolution time t the final state is the same as the state after the gate action. However, for the NMR Hamiltonian one would have to wait a time $t_1 > t$, where t_1 is given by the adiabatic condition, to implement the **Z**.

Bibliography

[1] Richard P Feynman. Simulating physics with computers. *International Journal of Theoretical Physics*, 21(6):467–488, 1982.

[2] David Deutsch. Quantum theory, the church-turing principle and the universal quantum computer. In *Proceedings of the Royal Society of London A: Mathematical, Physical and Engineering Sciences*, volume 400, pages 97–117. The Royal Society, 1985.

[3] Sergio Boixo, Sergei V Isakov, Vadim N Smelyanskiy, Ryan Babbush, Nan Ding, Zhang Jiang, John M Martinis, and Hartmut Neven. Characterizing quantum supremacy in near-term devices. *arXiv preprint arXiv:1608.00263*, 2016.

[4] Peter W Shor. Algorithms for quantum computation: Discrete logarithms and factoring. In *Foundations of Computer Science, 1994 Proceedings., 35th Annual Symposium on*, pages 124–134. Ieee, 1994.

[5] David Deutsch and Richard Jozsa. Rapid solution of problems by quantum computation. In *Proceedings of the Royal Society of London A: Mathematical, Physical and Engineering Sciences*, volume 439, pages 553–558. The Royal Society, 1992.

[6] Lov K Grover. A fast quantum mechanical algorithm for database search. In *Proceedings of the twenty-eighth annual ACM symposium on Theory of computing*, pages 212–219. ACM, 1996.

[7] H Dieter Zeh. On the interpretation of measurement in quantum theory. *Foundations of Physics*, 1(1):69–76, 1970.

[8] C Negrevergne, TS Mahesh, CA Ryan, M Ditty, F Cyr-Racine, W Power, N Boulant, T Havel, DG Cory, and R Laflamme. Benchmarking quantum control methods on a 12-qubit system. *Physical Review Letters*, 96(17):170501, 2006.

[9] Marco A Pravia, Evan Fortunato, Yaakov Weinstein, Mark D Price, Grum Teklemariam, Richard J Nelson, Yehuda Sharf, Shyamal Somaroo, CH Tseng, Timothy F Havel, et al. Observations of quantum dynamics by solution-state nmr spectroscopy. *arXiv preprint quant-ph/9905061*, 1999.

[10] Isaac L Chuang, Neil Gershenfeld, Mark G Kubinec, and Debbie W Leung. Bulk quantum computation with nuclear magnetic resonance: theory and experiment. In *Proceedings of the Royal Society of London A: Mathematical, Physical and Engineering Sciences*, volume 454, pages 447–467. The Royal Society, 1998.

[11] Max Born and Vladimir Fock. Beweis des adiabatensatzes. *Zeitschrift für Physik A Hadrons and Nuclei*, 51(3):165–180, 1928.

[12] Tosio Kato. On the adiabatic theorem of quantum mechanics. *Journal of the Physical Society of Japan*, 5(6):435–439, 1950.

[13] Tameem Albash and Daniel A Lidar. Adiabatic quantum computing. *arXiv preprint arXiv:1611.04471*, 2016.

[14] MHS Amin, CJS Truncik, and DV Averin. Role of single-qubit decoherence time in adiabatic quantum computation. *Physical Review A*, 80(2):022303, 2009.

[15] Michael V Berry. Quantal phase factors accompanying adiabatic changes. In *Proceedings of the Royal Society of London A: Mathematical, Physical and Engineering Sciences*, volume 392, pages 45–57. The Royal Society, 1984.

[16] Alan C Santos and Marcelo S Sarandy. Generalized shortcuts to adiabaticity and enhanced robustness against decoherence. *arXiv preprint arXiv:1702.02239*, 2017.

[17] Seth Lloyd et al. Universal quantum simulators. *SCIENCE-NEW YORK THEN WASHINGTON-*, pages 1073–1077, 1996.

[18] Michael A Nielsen and Isaac Chuang. Quantum computation and quantum information, 2002.

[19] Stephen Barnett. *Quantum information*, volume 16. Oxford University Press, 2009.

[20] Xiaoguang Wang, Chang-Shui Yu, and XX Yi. An alternative quantum fidelity for mixed states of qudits. *Physics Letters A*, 373(1):58–60, 2008.

[21] Charles P Slichter. *Principles of magnetic resonance*, volume 1. Springer Science & Business Media, 2013.

[22] Ivan Oliveira, Roberto Sarthour Jr, Tito Bonagamba, Eduardo Azevedo, and Jair CC Freitas. *NMR quantum information processing.* Elsevier, 2011.

[23] Felix Bloch. Nuclear induction. *Physical Review*, 70(7-8):460, 1946.

[24] Frederic A Hopf, Robert F Shea, and Marlan O Scully. Theory of optical free-induction decay and two-photon superradiance. *Physical Review A*, 7(6):2105, 1973.

[25] John E Tanner and Edward O Stejskal. Restricted self-diffusion of protons in colloidal systems by the pulsed-gradient, spin-echo method. *The Journal of Chemical Physics*, 49(4):1768–1777, 1968.

[26] Erwin L Hahn. Spin echoes. *Physical Review*, 80(4):580, 1950.

[27] Joseph B Altepeter, Daniel FV James, and Paul G Kwiat. 4 qubit quantum state tomography. In *Quantum state estimation*, pages 113–145. Springer, 2004.

[28] Edward Farhi, Jeffrey Goldstone, Sam Gutmann, Joshua Lapan, Andrew Lundgren, and Daniel Preda. A quantum adiabatic evolution algorithm applied to random instances of an np-complete problem. *Science*, 292(5516):472–475, 2001.

[29] Dave Bacon and Steven T Flammia. Adiabatic gate teleportation. *Physical Review Letters*, 103(12):120504, 2009.

[30] Jiangfeng Du, Lingzhi Hu, Ya Wang, Jianda Wu, Meisheng Zhao, and Dieter Suter. Is the quantum adiabatic theorem consistent? *arXiv preprint arXiv:0801.0361*, 2008.

[31] Jiangfeng Du, Lingzhi Hu, Ya Wang, Jianda Wu, Meisheng Zhao, and Dieter Suter. Experimental study of the validity of quantitative conditions in the quantum adiabatic theorem. *Physical Review Letters*, 101(6):060403, 2008.

[32] Mustafa Demirplak and Stuart A Rice. Adiabatic population transfer with control fields. *The Journal of Physical Chemistry A*, 107(46):9937–9945, 2003.

[33] Mustafa Demirplak and Stuart A Rice. Assisted adiabatic passage revisited. *The Journal of Physical Chemistry B*, 109(14):6838–6844, 2005.

[34] Leslie E Ballentine. *Quantum mechanics: a modern development.* World Scientific, 1998.

[35] Daniel Comparat. General conditions for quantum adiabatic evolution. *Physical Review A*, 80(1):012106, 2009.

[36] Alan C Santos and Marcelo S Sarandy. Superadiabatic controlled evolutions and universal quantum computation. *Scientific Reports*, 5:15775, 2015.

[37] Alan C Santos, Raphael D Silva, and Marcelo S Sarandy. Shortcut to adiabatic gate teleportation. *Physical Review A*, 93(1):012311, 2016.

[38] Erik Torrontegui, Sara Ibánez, Sofia Martínez-Garaot, Michele Modugno, Adolfo del Campo, David Guéry-Odelin, Andreas Ruschhaupt, Xi Chen, Juan Gonzalo Muga, et al. Shortcuts to adiabaticity. *Adv. At. Mol. Opt. Phys*, 62:117–169, 2013.

[39] Marcela Herrera, Marcelo S Sarandy, Eduardo I Duzzioni, and Roberto M Serra. Nonadiabatic quantum state engineering driven by fast quench dynamics. *Physical Review A*, 89(2):022323, 2014.

[40] Xi Chen, I Lizuain, A Ruschhaupt, D Guéry-Odelin, and JG Muga. Shortcut to adiabatic passage in two-and three-level atoms. *Physical Review Letters*, 105(12):123003, 2010.

[41] DM Tong, K Singh, Leong Chuan Kwek, and Choo Hiap Oh. Quantitative conditions do not guarantee the validity of the adiabatic approximation. *Physical Review Letters*, 95(11):110407, 2005.

[42] Karl-Peter Marzlin and Barry C Sanders. Inconsistency in the application of the adiabatic theorem. *Physical Review Letters*, 93(16):160408, 2004.

[43] Zhaoyan Wu and Hui Yang. Validity of the quantum adiabatic theorem. *Physical Review A*, 72(1):012114, 2005.

[44] Andrzej Ejchart, Pawel Oleski, and Krzysztof Wróblewski. Extended inversion-recovery method for spin-lattice relaxation measurements. a key to accurate t1 determination. *Journal of Magnetic Resonance (1969)*, 68(2):207–216, 1986.

[45] Ray Freeman. Selective excitation in high-resolution nmr. *Chemical Reviews*, 91(7):1397–1412, 1991.

[46] Lieven MK Vandersypen and Isaac L Chuang. Nmr techniques for quantum control and computation. *Reviews of Modern Physics*, 76(4):1037, 2005.

[47] Joseph P Hornak. The basics of mri, 1996.

[48] Jae-Seung Lee. The quantum state tomography on an nmr system. *Physics Letters A*, 305(6):349–353, 2002.